Title: Titan Mice are Unique Short-Lived mammalian model of metabolic syndrome and aging

Authors: Irene de-Diego[1†], Adrián Sanz-Moreno[2†], Annika Müller-Eigner[1†], Anuroop Venkateswaran Venkatasubramani[3], Martina Langhammer[4], Raffaele Gerlini[2,5], Birgit Rathkolb[2,5,6], Antonio Aguilar-Pimentel[2], Tanja Klein-Rodewald[2], Julia Calzada-Wack[2], Lore Becker[2], Axel Imhof[3], Chen Meng[7], Christina Ludwig[7], Franziska Koch[8], Eliana von Krusenstiern[9], Erika Varner[9], Nathaniel W. Snyder[9], Vanessa Caton[10], Julia Brenmoehl[10], Andreas Hoeflich[10], Helmut Fuchs[2], Valerie Gailus-Durner[2], Martin Hrabe de Angelis[2,5,11] and Shahaf Peleg[1*]

Affiliations:

[1]Research Group Epigenetics, Metabolism and Longevity, Leibniz Institute for Farm Animal Biology, 18196 Dummerstorf, Germany
[2]German Mouse Clinic, Institute of Experimental Genetics, Helmholtz Zentrum Munich, German Research Center for Environment and Health (GmbH), 85764 Neuherberg, Germany
[3]Department of Molecular Biology, Biomedical Center Munich, Ludwig-Maximilians University, Großhaderner Strasse 9, 82152 Planegg-Martinsried, Germany
[4] Institute Genetics and Biometry, Lab Animal Facility, Leibniz Institute for Farm Animal Biology, 18196 Dummerstorf, Germany
[5]German Center for Diabetes Research (DZD), 85764 Neuherberg, Germany
[6]Institute of Molecular Animal Breeding and Biotechnology, Gene Center, Ludwig-Maximilians-University München, Feodor-Lynen Str. 25, 81377 Munich, Germany
[7]Bavarian Center for Biomolecular Mass Spectrometry, Technical University of Munich, 85354, Freising, Germany
[8]Institute of Nutritional Physiology, Leibniz Institute for Farm Animal Biology, 18196 Dummerstorf, Germany
[9]Center for Metabolic Disease Research, Department of Microbiology and Immunology, Lewis Katz School of Medicine Temple University, Philadelphia, PA, 19140 USA
[10]Institute for Genome Biology, Leibniz Institute for Farm Animal Biology, 18196 Dummerstorf, Germany
[11]Chair of Experimental Genetics, School of Life Science Weihenstephan, Technische Universität München, 85354 Freising, Germany

*Correspondence: shahafpeleg3@googlemail.com or peleg@fbn-dummerstorf.de

† These authors contributed equally.

Summary:

Metabolic syndrome is widespread and negatively impacts healthy longevity but takes years to study in mammalian models, delaying translational applications. To address this, we characterized the unique polygenic “Titan” mouse (110 grams average) with a healthy lifespan of only 4 months that was generated by 45 years of breeding selection. Titan mice displayed increased plasma leptin, insulin, IL-6 and fasting triglycerides. Also, pancreatic fat cell accumulation and thymic medullary hyperplasia were detected in Titan animals. Liver transcriptome and proteome analysis demonstrated alterations in lipid metabolism, the methionine cycle, and cytochrome P450 regulation in Titan mice. Late dietary intervention in Titan mice reduced fat content and improved expression of genes involved in lipid synthesis and cytochrome P450 detoxification, altering the abundance of metabolites, including malonyl-CoA and dimethylglycine. Strikingly, late dietary intervention at 3 months of age almost doubled the healthy lifespan of Titan mice. This powerful model of metabolic disorders, systemic inflammation, and early aging will enable to provide uniquely rapid results for translational intervention.

Introduction:

Improvements in public health and quality of life have increased life expectancy, with a concomitant increase in age-related diseases (Crimmins, 2015; Nikolich-Žugich et al., 2016) caused by progressive deterioration of tissue structure and function(López-Otín et al., 2013). Age-related pathologies, such as cancer and neurodegenerative, autoimmune, cardiovascular, and metabolic diseases [e.g., metabolic syndrome (MetS) (López-Otín et al., 2016), cause major morbidity and mortality (López-Otín et al., 2016). MetS is especially quite prevalent in middle-aged people in the western world (Bonomini et al., 2015; Hildrum et al., 2009; Lund et al., 2020; Monteiro and Azevedo, 2010; WHO, 2020). Thus, targeting the onset and progression of MetS to promote healthy aging will benefit a large and growing demographic.

Short-lived non-mammalian model organisms such as worms, flies, and killifish (Kenyon, 2010; Longo et al., 2015; Poeschla and Valenzano, 2020) have provided substantial insight into the molecular mechanisms of metabolic aging potentially informing novel healthy lifespan-extending therapies, but data from these organisms may not be generalizable to understand and intervene in human aging. Mammalian models are more closely related to humans but require expensive and time-consuming research, with results sometimes achievable only after several years (Kõks et al., 2016; Li and Auwerx, 2020; Liao and B. K. Kennedy, 2014; Yuan et al., 2009). For a more timely and reasonable experimental design, inbred mouse lines with accelerated aging (Liao and B. K. Kennedy, 2014; Yuan et al., 2009) have been created by generating targeted point-mutations in specific pathways relevant to aging. This approach allows studying the relative contribution of each component of the

aging process. In this respect, several progeroid mouse models engineered with mutations affecting genomic stability have been generated (Folgueras et al., 2018; Liao and B. K. Kennedy, 2014). Likewise, lines with deficiencies in specific metabolic genes have been created to model MetS (A. J. Kennedy et al., 2010), a major syndrome affecting healthy aging (A. J. Kennedy et al., 2010), particularly leptin-deficient ($Lep^{ob/ob}$) (Y. Zhang et al., 1994), leptin receptor-deficient ($LepR^{db/db}$), and lethal yellow agouti (A^{y}/a) mice (A. J. Kennedy et al., 2010).

Currently, such in-bred mouse lines are the most commonly used mammalian models to study aging (Yuan et al., 2009) (Kõks et al., 2016; Li and Auwerx, 2020). However, these models have several drawbacks, as aging is a multifactorial process with multiple genes having combined effects on an organism's lifespan(López-Otín et al., 2013). Therefore, inbred lines carrying specific genetic mutations may not reflect the more variable metabolic aging of humans (Li and Auwerx, 2020). Further, many common inbred mouse models, such as C57BL/6J, have specific genomic alterations (e.g., deletions in coding regions) as well as extremely long telomeres coupled with higher telomerase activity in many organs, which can give rise to non-generalizable results(Calado and Dumitriu, 2013). Alterations in such key biological processes impose obstacles for interpreting data in the context of other organisms. Thus recently, the disadvantages of using extreme standardization (i.e., use of specific inbred mice) have been emphasized (Li and Auwerx, 2020). Furthermore, the outcome of lifespan interventions may differ between various inbred mice, producing conflicting results (Liao et al., 2010) and inhibiting transfer of this knowledge to

the more diverse human population (Li and Auwerx, 2020). Therefore, using out-bred mice may be more relevant to develop interventions in human aging.

The Dummerstorf non-inbred mouse line “Titan” (previously called DU6), a giant mouse (110 grams average) strain created over 45 years via >180 generations of weight-based breeding selection (Bünger et al., 1998; Renne et al., 2013; Timtchenko et al., 1999), is a potential alternative model for defects in metabolic aging. These mice are polygenic and characterized by gigantism, obesity, increased growth hormone levels (GH), and possible alterations in fat metabolism (Liao and B. K. Kennedy, 2014; López-Otín et al., 2013). Of interest, the GH - insulin-like growth factor 1 signalling (IIS) axis, which mediates mammalian growth and metabolism, represents perhaps the most potent and best characterized pathway involved in longevity

(Altintas et al., 2016; Lee and Longo, 2018). For example, transgenic mice overexpressing different GH genes live much shorter than the wild-type controls (Bartke, 2003; Steger et al., 1993).

We hypothesized that giant Titan mice would display a shorter lifespan than control mice (Bartke, 2003). Overall, we aimed to characterise metabolic changes in Titan mice and decipher how such alterations may impact their lifespan by combining histological and plasma analysis with liver RNA sequencing and proteome analysis. We also used these mice to explore interventions that may be applicable to promote healthy aging. Our findings support the use of these mice as a suitable efficient polygenic model for study of the complexities inherent in metabolic aging.

Results

45 years of body weight selection to create Titan mice

Ongoing selection over the past 180 generations has caused profound changes in the phenotype of the non-inbred Titan line. Unselected control and Titan mice average 35 and 90 g at the age of selection (6 wks), respectively (Figure 1A and B). Controls reach an average of 45 g by 4 months. Six-week old Titan mice display a considerably bigger size than unselected mice (Figure 1B). At 10–11 wks of age, Titan mice reach 14.75 cm in body length (Figure 1C) and exhibit an increase in both total fat and lean mass as well as fat percentage (Figure 1D and E). Of note, fat distribution is also altered, with Titan mice accumulating more intra-abdominal fat than controls (Figure 1F).

Previous studies have described an inverse link between size, BMI, and longevity within a species(Selman et al., 2013), so it seemed intriguing that the lifespan of Titan mice might differ from controls. Indeed, the lifespan of Titan mice was dramatically shorter than the outbred control strain (Figure 1G). Titan mice reached the pre-mortality plateau phase (10% death) at 4–5 months, while controls reached theirs at 10 months. The mean survival time was also strikingly different, with 50% of Titan mice dying by around 10 months of age. Also, by 4 months of age, Titan mice grow to an average of 115 g (Figure 1H) and their skeletons are larger than those of controls (Figure 1I). In terms of experimental length and selection success, this ongoing experiment represents a unique scientific endeavor and, to our knowledge, has produced the largest known mouse model (A. J. Kennedy et al., 2010).

Based on the pre-mortality plateau data, we compared various parameters in Titan and control mice at 4–5 months (16–17 wks, 110–120 days) of age to determine what factors might underlie the different lifespans of these strains. The following sections describe data collected from this age unless otherwise stated. Alterations (e.g., changes in histopathology and other parameters) in several tissues as well as blood and plasma markers were examined using the German Mouse Clinic (GMC) standardized techniques(Gailus-Durner et al., 2005).

Titan mice have altered fat metabolism

Titan mice not only accumulated more intra-abdominal fat than controls (Figure 1F), but also showed substantial whitening of brown adipose tissue (BAT) (Figure 2A and S1). By contrast, control mice showed no BAT whitening (Figure S1). Such whitening of adipose tissue has recently been linked to inflammation and may contribute to the low-grade inflammatory state observed in obesity and aging (Kotzbeck et al., 2018). Titan mice also showed multifocal fatty cells in the pancreas without atrophic or inflammatory changes of the adjacent parenchyma, a phenotype not present in control mice (Figure 2B and S2). Although pancreatic lipomatosis has been poorly investigated compared to hepatic lipomatosis, it is a common pathological condition that can be considered an early marker of MetS (Catanzaro et al., 2016) and that strongly correlates with obesity, aging, and dyslipidaemia. We also found that leptin levels, a hormone secreted by adipocytes (Guilherme et al., 2019; A. J.

Kennedy et al., 2010; Lund et al., 2020) that modulates food intake and fat storage, were significantly increased in Titan mice (Figure 2C).

Fasting plasma levels of triglycerides, non-HDL, HDL, and total cholesterol were significantly higher in Titan mice than control mice (Figure S3). Non-HDL/HDL ratio was increased in Titan mice, suggesting the increase in non-HDL was more pronounced than HDL. Notably, these differences in lipid levels between Titan and control lines were larger in younger (10–11-wk old) mice (Figure S3). Hyperlipidemia usually occurs in the presence of insulin resistance, as insulin regulates lipid metabolism (Saltiel and Kahn, 2001) and promotes cholesterol uptake in intestinal epithelial cells (Fuentes et al., 2018). Consistent with this, insulin levels were higher but glucose concentrations were similar in Titan and control mice (Figure 2D and E), indicating a lower sensitivity to insulin resistance in Titan mice (Wilcox, 2005).

In addition, fibroblast growth factor 21 was elevated in Titan mice, which may further indicate metabolic deregulations (Figure 2F). Elevated FGF21 levels may associate with MetS (X. Zhang et al., 2008) and correlate with type 2 diabetes (Cheng et al., 2011) and non-alcoholic fatty liver disease (Yan et al., 2011). Finally, Titan mice displayed higher alpha amylase activity, which may imply increased production in the liver or impaired renal clearance (Figure 2G).

In sum, the combination of high fat, high fasting triglyceride levels, high cholesterol, and insulin resistance support the notion that Titan mice may develop MetS (Bonomini et al., 2015; A. J. Kennedy et al., 2010), possibly contributing to their shorter lifespans.

Titan mice display signs of systemic inflammation and tissue damage

A major hallmark of aging is the rise of systemic inflammation (Fulop et al., 2014; López-Otín et al., 2013; Stepanova et al., 2015). Inflammation is a common factor between many age-related diseases, from cancer to metabolic, autoimmune, and neurodegenerative maladies. Chronic inflammation or "inflammaging" markers are significant predictors of mortality in humans (Candore et al., 2010; Franceschi and Campisi, 2014) and linked to MetS (Monteiro and Azevedo, 2010).

To evaluate if inflammation is altered in Titan mice, we measured inflammation indicators in plasma. We found that interleukin 6 (IL6) and tumour necrosis factor-alpha (TNFα), cytokines central to inflammation, were significantly increased in Titan mice (Figure 3A and B). Interestingly, both TNFα and IL6 are overexpressed in the adipose tissue of obese mice and in humans (Popko et al., 2010; Pradhan et al., 2001), providing a link between obesity, diabetes and chronic inflammation. As an additional sign of inflammation, histological analysis of the thymus revealed the presence of nodular thymic medullary hyperplasia in Titan mice (Figure 3C and S4). Immunohistochemistry of these medullar nodes revealed that they are composed mainly of B-cells (Figure 3C and S5). Formation of follicular-like B-cell aggregates is considered a sign of thymic involution, a gradual, non-reversible change occurring during aging (Pearse, 2006). Importantly, nodular thymic medullary hyperplasia is also seen in autoimmune disorders (Leite et al., 2007; Ward et al., 2012). Further alterations of plasma factors that may correlate with other inflammatory markers were found in Titan mice. For example, plasma levels of alkaline

phosphatase (ALP), a possible indicator for cholestasis or bone metabolism alterations, were increased (Figure 3D).

Furthermore, alanine aminotransferase (ALAT) activity, a marker usually indicative of liver damage but also with mild elevations in cases of gallbladder blockage, overactive parathyroid gland, muscle damage, renal failure, or bone disease (Gowda et al., 2009; Malakouti et al., 2017), was elevated in Titan mice (Figure 3E). However, no clear signs of hepatocellular disease were found in histological analysis by H&E staining of Titan liver tissue (Figure S6). Despite this, Oil red O staining of the liver revealed increased fat content in Titan mice (Figure 3F). Bilirubin, a waste product of heme metabolism that can be toxic in individuals with liver disease but also exhibits antioxidant and anti-inflammatory effects at normal levels (Frei et al., 1988), was significantly lower in older Titan mice compared to controls (Figure 3G). In addition, Titan plasma urea levels were lower than controls, pointing to possible dysregulation of protein metabolism and the urea cycle in the liver (Figure 3H). Of note, Titan mice have excess iron in plasma along with low unsaturated iron binding capacity, resulting in reduced total iron binding capacity and increased transferrin saturation (Figure S7). Hyperferritinemia is common in humans with MetS (L. Y. Chen et al., 2011) as well as liver dysfunction (Senjo et al., 2018).

Kidney histology revealed the presence of basophilic tubules and tubular casts in half of the Titan mice analyzed (Figure S8). Further, we observed elevated plasma electrolytes and mineral levels such as potassium, calcium, and inorganic phosphate, which might be due to impaired renal tubular function (Figure S9). We also detected fibrotic tissue in the hearts of 3/6 of 15–17-wk old Titan mice and in 5/6 of 25–26-wk old Titan mice (Figure S10).

Altogether, the Titan mice appear to have an altered communication between fat, pancreas and liver, which leads to a dysfunctional metabolism with signs of MetS and premature aging. Dysregulation of energy homeostasis is highly related to inflammation and it is likely to cause further damage to other systems. Several markers indicate a generalized altered function in liver and kidneys of Titan mice, which co-occur with high levels of systemic inflammation.

Liver transcriptome and proteome indicate metabolic alterations in Titan mice

To better understand the altered metabolism of Titan mice, we performed RNA sequencing on liver from 11-wk old and 19–21-wk old Titan and control mice. Principal component analysis (PCA) revealed distinct Titan and control transcriptomes (Figure 4A). Gene expression in younger and older controls also clustered together, but for Titan mice, the expression profile shifted with age (Figure 4A).

Compared to age-matched controls, young Titan mice exhibited upregulation of 1150 and downregulation of 1227 genes (Figure 4B and S11A). Pathway enrichment analysis revealed upregulation of many genes involved in fat, lipid and various metabolic pathways e.g., *mTOR, Elovl5, Elovl6*, and acetyl-CoA carboxylase (*Acaca*). Various downregulated genes were associated with xenobiotic metabolism (Figure 4C). Many genes from the cytochrome P450 family were downregulated in young Titan mice as well as genes involved in several metabolic processes such as unsaturated fatty acid, glutathione, and other relevant pathways (Figure 4C). Previous work has linked downregulation

of cytochrome P450 genes in the liver to higher inflammation (Morgan, 2009; Siewert et al., 2000). Cytochrome P450 enzymes also metabolize endogenous metabolites (Lewis, 2004). Of note, various genes related to methionine and folate cycle pathways [e.g., *Bhmt, Gnmt, Cth* (*Cgl*), *Dmgdh*] were downregulated in Titan mice.

There were only minor changes in gene expression (52 genes) when comparing young and old control mice, but intragroup variability of Titan mice was significantly higher, making it possible to differentiate between the two age groups (Figure 4B). Older Titan mice had 146 upregulated genes and 257 downregulated genes (Figure S11B). Thus, Titan mice displayed early transcriptomic changes during aging. For example, the aged group had increased expression of enzymes involved in glucose and insulin response were also upregulated in the old Titan group (Figure S11C), but fatty acid synthesis, coenzyme metabolism, and other metabolic pathways were downregulated (Figure S11C), including marked downregulation of *Acaca*. Interestingly, *Cyp7b1*, which codes for an enzyme involved in cholesterol catabolism that converts cholesterol to bile acids, was upregulated in older Titan mice. Overexpression of CYP7B1 is implicated in osteoarthritis, and such joint diseases are exacerbated by excess body weight (Choi et al., 2019).

Some pathways upregulated when comparing young Titan and control mice declined in older Titan mice. This is reflected by direct comparison of older Titan and control mice. The number of altered genes in older groups (1521 different genes compared to control) was lower than for younger groups (2377 genes) (Figure 4B and S11D). In particular, we found 693 upregulated genes in old Titan mice, the majority involved in various pathways regulating cell

development and neuronal activity, whereas 828 genes were downregulated (Figure 4D). Compared to old control mice, old Titan mice exhibited lower gene expression within various metabolic pathways (e.g., amino acid metabolism) and lower xenobiotic gene expression. Notably, many of the genes altered when comparing young mice were also altered when comparing older mice, with 402 upregulated (out of 693) and 461 downregulated genes (out of 828) in comparisons of young Titan to control and old Titan to control mice. Respective to age-matched controls, both young and old Titan mice had reduced expression of many genes in the cytochrome P450 family.

To complement the transcriptome study, we compared the liver proteomes of Titan and control mice. Similar to RNAseq data, larger proteomic changes were seen in the young Titan to control comparison than the old comparison (Figure 5A and C). Relative to age-matched controls, young Titan mice exhibited 207 upregulated and 289 downregulated proteins, while old Titan mice showed 125 upregulated and 142 downregulated proteins (Figure 5A and C, see analysis cut-off in method section). Also, similar to transcriptome results, pathway analysis revealed increased fatty acid synthesis in young Titan mice (Figure 5B). In particular, fat utilization (enrichment of proteins such as ACACA, IDH1, and ACOX1) as well as lipid biosynthesis (FASN, ACLY, and ACSL5,) were enhanced, which might explain increased plasma cholesterol and triglyceride levels in these mice (Figure S3). Similar changes have been observed in the liver during MetS (Ayoub et al., 2018; Hsieh et al., 2016) and aging (Houtkooper et al., 2011). Interestingly, proteins involved in lipid metabolism were not obviously enriched when old Titan mice were compared to age-matched controls (Figure 5D). Proteins upregulated in old Titan mice were linked to

lysosome activity (Figure 5D), and downregulated proteins were enriched in various metabolic pathways, e.g., folate metabolism (Figure 5D). Similar to transcriptome data, we observed a reduction in the abundance of BHMT, GNMT, and CTH (CGL), key proteins in the methionine cycle.

Both our transcriptome and proteome data revealed substantial changes in liver metabolism between Titan and control mice. Further, and consistent with Figure S3, those changes were more dramatic in younger mice. We observed a substantial albeit incomplete overlap between factors identified in our transcriptomic and proteomic analyses consistent with previous observations on these two techniques (Figure S12) (Maier et al., 2009). The fact that many altered genes were not detected in the single shot proteome analysis can be attributed to the lower relative coverage of the proteome approach (Maier et al., 2009).

Protein abundance causes metabolic alterations, but posttranslational modifications of proteins can also affect this process(Choudhary et al., 2014). Specifically, protein acetylation is involved in metabolic regulation and various other cellular pathways (Choudhary et al., 2014). We compared the acetylome of young Titan to young control mice, analysing acetylation differences at 816 sites that met the cut-off criteria (Figure S13A; see methods for cut-off criteria). In total, 134 acetylation sites were differentially modified: 117 sites were decreased while only 17 were increased in Titan mice (Figure S13B and C). Pathway analysis revealed that many hypo-acetylated proteins localize to mitochondria and participate in translation and metabolic processes such as glycine and serine metabolism (Figure S13C). For example, ACSL1, which converts long chain fatty acids into fatty acyl-CoA, and various ATP synthase

subunits were hypoacetylated. BHMT, GNMT, and CTH (CGL), proteins involved in the methionine cycle, had reduced mRNA (Figure 4), protein (Figure 5), and relative acetylation levels (Figure S13A). The only pathway enriched in hyperacetylated proteins in Titan mice was lipid metabolism, although the number of proteins enriched in this pathway was modest (Figure S13B). Our data suggest a moderate shift to lower protein acetylation in young Titan mice, which may underlie several metabolic changes.

Late dietary intervention at 12 weeks doubles the pre-mortality plateau phase in Titan mice

Dietary intervention, intermittent fasting, or restriction of a specific macronutrient (i.e., proteins) is a well-studied and robust intervention that extends lifespan in various animal models (Di Francesco et al., 2018; Fontana and Partridge, 2015; Greer and Brunet, 2009; Kenyon, 2010; Longo et al., 2015; Miller et al., 2017; Puca et al., 2008). However, not all mouse strains are responsive to caloric reduction (Li and Auwerx, 2020; Liao et al., 2010), and actually most have a negative response (Liao et al., 2010).

To analyse the impact of a dietary intervention on the lifespan of Titan mice, we used a healthy diet with moderate energy reduction (ERF; see methods). Remarkably, late ERF intervention at 84 days of age almost doubled the pre-mortality plateau phase (>90% survival) in Titan mice (Figure 6A). However, the reduced-energy diet eventually had only limited effect on the death rate at 270 days, which was 30% in both ERF and control groups. Beyond, 270 days, ERF increased lifespan (Figure 6A). Starting at day 84, ERF-fed male Titan mice

weighed 5–10% less than their control male siblings (Figure 6B), and by day 147, ERF-fed mice had significantly reduced abdominal fat weight (Figure 6C).

ERF intervention at 12 wks of age altered mRNA levels by 21 wks of several enzymes in the methionine cycle (Figure 6D), which were already identified in our -omics experiments as being lower in young Titan compared to control mice (Figure 4 and 5). Further, late ERF intervention reversed the age-dependent deregulation of *Cyp7b1* and *Acaca* in Titan mice (Figure 6D). ERF intervention also resulted in increased levels of liver malonyl-CoA, which is synthesized by ACACA, without affecting levels of other CoAs (Figure 6E). A recent study using mutant malonyl CoA decarboxylase mice found that higher malonyl-CoA correlates with increased lifespan (Ussher et al., 2016). In addition, both serum and intra-abdominal fat levels of dimethylglycine (DMG) and adenosine were increased in response to ERF (Figures 6F and S14).

The above results support the notion that a late ERF intervention causes transcriptional, metabolic, and physiological alterations linked to an increase in healthy lifespan in Titan mice.

Discussion

This study provides an unprecedented and in-depth analysis of the giant short-lived mouse line Titan, a possible non-inbred model for metabolic syndrome (MetS) and metabolic aging. The molecular phenotype of these mice shows several hallmarks associated with MetS, including a combination of high fat and obesity (Grundy et al., 2005; A. J. Kennedy et al., 2010). Additionally, alterations in the Titan liver transcriptome and proteome appear to contribute

to MetS, and our data show several relevant markers for this condition (Grundy et al., 2005). As expected, Titan mice are short-lived and show early signs of aging, including systemic inflammation, presence of B cells in thymic medullar nodes, and cardiac fibrosis. Unlike commonly used MetS mouse models, Titan mice have intact leptin signalling, making them an interesting and novel model for this disease (A. J. Kennedy et al., 2010). Unlike $Lep^{ob/ob}$ mice that possess poor fertility (A. J. Kennedy et al., 2010), Titan mice are relatively easy to maintain and can provide sufficient numbers for various large studies.

Titan mice have many circulating markers for metabolic dysfunction. For example, they display high fasting triglyceride levels, non-HDL cholesterol, and high non-HDL/HDL ratio that are strongly linked to atherosclerosis and cardiovascular disease, especially in the presence of systemic inflammation (Gimbrone and García-Cardeña, 2016; Libby, 2002; Ridker et al., 2017). However, HDL cholesterol is traditionally regarded as protective (Assmann and Gotto, 2004). Indeed, dyslipidaemia in MetS is characterized by low fasting HDL levels (Grundy et al., 2005), although this not necessarily true in mouse models of MetS (A. J. Kennedy et al., 2010). Nevertheless, HDL cholesterol is controlled by multiple genetic and environmental factors (Zannis et al., 2015), so high levels in obese organisms such as Titan mice should be interpreted with caution. HDL particles can also exert negative effects (Alwaili et al., 2012), particularly in the presence of mutations that target formation and clearance of HDL particles (Asztalos et al., 2011). In addition to lipid markers, we found elevated plasma electrolytes and minerals (e.g., potassium, calcium, and inorganic phosphorus), indicating possible impaired renal tubular function. In regards to kidney function, increased plasma cholesterol levels, observed in

fasting as well as ad libitum fed states, can be a secondary consequence of proteinuria (Agrawal et al., 2017).

An important feature linked with MetS and aging in humans is excessive accumulation of visceral fat, which is regarded as a major culprit in insulin resistance (Grundy et al., 2005; Hardy et al., 2012; Hunter et al., 2010; Shah et al., 2014). Titan mice also display higher levels of intra-abdominal fat, which correlates with hyperinsulinemia, whitening of BAT, and fat cells presence in the pancreas. BAT whitening is strongly linked to obesity (Kotzbeck et al., 2018) and becomes more prevalent during aging in both humans and rodents (Zoico et al., 2019). As mice age, small lipid droplets normally observed in brown adipocytes coalesce into a single vacuole (Brayton et al., 2012), as observed in Titan mice.

Our data support a link between obesity, diabetes, and chronic inflammation. Our mice have several markers of systemic inflammation and tissue damage, such as high levels of IL6 and TNFα, thymic medullary hyperplasia, and other liver and kidney disease markers. TNFα activity is tightly linked to other cytokines such as IL1 and the IL6 family. Dysregulation of these pathways is implicated in onset and maintenance of several diseases (Heinrich et al., 2003; Landskron et al., 2014) and both TNF α and IL6 are overexpressed in adipose tissue of obese mice and in humans (Popko et al., 2010; Pradhan et al., 2001). Further, previous work showed a strong causal link between higher IL6 levels and MetS (Mohammadi et al., 2017; Weiss et al., 2013). Both cytokines are significant independent predictors of mortality in elderly humans (Brüünsgaard and Pedersen, 2003).

Transcriptomic and proteomic changes in the livers of Titan mice likely drive the above-mentioned phenotypes and affect healthy aging. At 11 wks, genes involved in lipid metabolism and biosynthesis were consistently upregulated in Titan mice, which might account for high levels of cholesterol and fasting triglycerides observed in this model. Interestingly, various methionine metabolism enzymes were also generally reduced in Titan mice. On the other hand, 11-wk-old Titan livers exhibited several downregulated genes and proteins associated with xenobiotic metabolism, such as cytochrome P450, indicating that Titan mice have a reduced capacity to deal with toxic compounds in the liver. Xenobiotic metabolism strongly impacts the ability of the organism to maintain homeostasis and cope with disease, which may contribute to the increased morbidity of these mice (Crocco et al., 2019).

One of the signaling pathways upregulated in 19–21-wk-old (older) Titan mice was linked with insulin response. Higher expression of these genes (e.g., *Enpp1*, *Tbc1d4*, *Enho*) may drive the observed plasma markers of altered glucose and energy metabolism in Titan mice. ENPP1 directly interacts with the α-subunit of the insulin receptor and modulates its intracellular signaling (Pan et al., 2012). Higher hepatic *Enpp1* expression was found in diabetic rabbits (Eller et al., 2006). TB1D4 is an important substrate for the key regulator AKT in glucose metabolism and is involved in GLUT4 translocation after insulin secretion. Higher *Tbc1d4* expression is found in pancreatic and adipose tissues of the high-fasting-glucose group of a porcine pre-diabetic model (Kristensen et al., 2015). ENHO is required for energy homeostasis (Grzegorzewska et al., 2018), and higher expression might be linked to its dysregulation in Titan mice during aging.

Surprisingly, many differences (in gene and protein expression in the liver, as well as in circulating factors in the plasma following fasting) when comparing young Titan and control mice were attenuated during aging, including insulin signalling (IIS) activity. Previous work has shown that GH is reduced in 6-wk-old Titan mice compared to 3-wk-old mice (Timtchenko et al., 1999). Of note, although insulin plasma levels are elevated (compared to control) in young Titan mice, this difference is attenuated during aging (Renne et al., 2013). Indeed, data from a previous longitudinal study show improved glucose tolerance in Titan mice as they age, even if fed a high-fat diet (Renne et al., 2013). Several reasons for this have been proposed (Renne et al., 2013), but causes remain unclear. One possibility is that, as mice age, individuals with higher damage and metabolic dysregulation have an increased risk of mortality; thus, the remaining “long-lived” population shows a relative improvement in metabolic parameters. However, only ~10% of mice died by the older timepoint defined in this study (19–21 wks). Another possibility is that, as Titan mice age, their gigantic size outstrips their molecular capacity, resulting in attenuation of lipid metabolism and other metabolic pathways (e.g., mTOR regulation during aging). Further experiments should use a longitudinal approach to study the evolution of each individual throughout their lifespan and segregate primary changes in metabolism from secondary effects.

Our data support the notion that Titan mice display a dysregulated metabolism with signs of MetS, systemic inflammation, tissue damage in various organs and accelerated metabolic aging. Furthermore, previous works showed that Titan mice display higher levels of GH (Timtchenko et al., 1999). Transgenic mice overexpressing GH exhibit high inflammatory markers, an adverse lipid

profile, and associated shortened lifespan. These mice also show attenuation of the IIS pathway during aging (Ding et al., 2011), and they show desensitization of insulin signalling with hyperinsulinemia and hyperglycemia. Of note, GH over-expression in mice leads to glomerulosclerotic lesions (Blutke et al., 2016) and severe reduction in life span (Bartke, 2003).

We suggest that the short lifespan observed in Titan mice is partially due to continuous generalized damage generated by high levels of inflammation, a main hallmark of aging, which can be triggered by an altered metabolism. As such, we propose that this mouse line could be a suitable model for time-efficient metabolic aging studies. A main advantage of the Titan mice is their short lifespan. Aging experiments can generate results in as little as 4–6 months, when mice reach the pre-mortality plateau (>90% survival). This makes them an efficient model to study aging and interventions to extend healthy lifespan. As proof of principle, we demonstrated that a common anti-aging strategy, ERF, doubled the pre-mortality plateau phase and considerably reduced intra-abdominal fat in Titan mice. Of note, we showed that late ERF intervention at 12 wks of age could either reverse age-associated transcriptional alterations genes coding for key enzymes such as *Acaca*, *Cyp7b1*, and *Cyp2c37* or upregulate gene expression of enzymes of the methionine cycle such as *Cth*, *Gnmt*, and *Dmdgh* that are lower in Titan mice than in controls.

Several of these genes have already been implicated in mediating the benefits of caloric restriction in inflammation and age-associated maladies. For example, recent work shows that CTH (CGL) mediates the dietary restriction response via H_2S production (Hine et al., 2015). Similarly, food reduction

increases GNMT levels, promotes energy homeostasis, and increases lifespan (Obata et al., 2014; Obata and Miura, 2015). Further, upregulation of CYP7B1, a cholesterol hydrolase, is associated with inflammation and osteoarthritis, a common age-associated degenerative joint disease (Choi et al., 2019). *Cyp7b1* expression increases as Titan mice age. Thus, reduction of *Cyp7b1* may mediate, in part, the ERF-induced lifespan increase in Titan mice. In addition, we observed that ERF substantially increased CYP2c37, a member of the cytochrome P450 family with lower expression in Titan mice than in controls. Thus, ERF intervention may improve xenobiotic metabolism (Chou et al., 1993).

In Titan mice, ERF also upregulated ACACA, reflecting increased levels of malonyl-CoA in these calorie-restricted mice. Mutant mice deficient for malonyl CoA decarboxylase have higher levels of malonyl-CoA, live longer, and are better protected against high-fat induced insulin resistance (Ussher et al., 2016). As such, increased malonyl-CoA is linked with decreased inflammation associated with insulin resistance, promoting health in mice (Samokhvalov et al., 2012; Ussher et al., 2016). Further, we observed increased DMG levels in both liver and fat tissue upon ERF intervention. A recent report has linked higher levels of DMG with reduced prevalence of collagen-induced arthritis and reduced inflammation in rats (Lawson et al., 2007). This might be a contributing factor to the increased lifespan of ERF-treated Titan mice. Metabolic changes in Titan mice suggest ERF promotes healthier metabolic activity that could underlie the substantial healthy lifespan increase in this model, which already displays high levels of systemic inflammation. Importantly, these results were obtained in 4–5 months, whereas the same intervention can take much longer in other mouse models (Li and Auwerx, 2020).

In summary, the Titan mouse line, a giant non-inbred line with high genetic diversity, was created over many generations of breeding and represents a remarkable scientific achievement. The phenotype of these mice, including their short lifespan, is a possible consequence of several genetic and epigenetic changes (Peleg et al., 2016b). Importantly, as non-inbred mice, Titan animals may better reproduce the genetic variability of human populations and thus might be a useful option for preclinical drug testing (Li and Auwerx, 2020). Further studies should use a longitudinal approach to monitor IIS activity and other senescence markers in Titan mice to better understand their developmental changes. In addition, future anti-aging interventions such as senolytic drugs may help determine if accumulation of senescent cells contributes to the accelerated mortality of Titan mice (Baker et al., 2016). This work provides the preliminary phenotypic data required to establish the Titan model as a novel tool for studying and potentially developing fairly rapid pharmaceutical interventions for metabolic disorders, systemic inflammation, and the aging process and provide the basis for broader spectrum follow-up studies.

Acknowledgments

We would like to thank our technician Verena Hofer-Pretz for performing many of the experiments for this study, as well as managing the laboratory conditions that enable this work. The authors thank Ines Müntzel, Karin Ullerich, Sabine Maibohm, Benita Lucht, Hildburg Meier from the mouse facility for the animal care and technical assistance. The authors also thank Erika Wytrwat for

technical support. The GMC would like to to thank the technicians and animal care takers involved in this project for their expert technical help. We also thank Franziska Hackbarth, Nina Lomp and Hermine Kienberger for their excellent laboratory assistance.

The study was supported by the Leibnitz society and by the German Federal Ministry of Education and Research (Infrafrontier grant 01KX1012 to MHdA); German Center for Diabetes Research (DZD) (MHdA), the Helmholtz Alliance 'Aging and Metabolic Programming, AMPro` (RG).

Author contributions

SP conceptualized the project. ML prepared all the mice work conducted the survival curves with the weight measurements and assisted with conceptualizing this work. ML also maintains the Dummerstorf selection line. ID-D and AW-W prepared the RNAseq. ID-D, AM-E and SP prepared the proteome and acetylome data. AS-M, RG, BR, AA-P, TK-R, JC-W performed mouse phenotyping tests and analyzed the data, LB supported data analyzes and manuscript preparation, CS coordinated and VG-D, HF and MHdA supervised the project at the GMC and conceived phenotyping test pipeline. AW-W analized the RNA-seq and generated the data visualization. AI supervised AW-W work. CM and CL ran, analyzed and visualized the proteome and acetylome data and. EvK, EV and NW-S prepared and analyzed the metabolites measurements. VC ad JB prepared and analyzed the Oil red O straining. AH supervised the work of VC and JB. ID-D, FC and SP wrote the

initial manuscript. All authors contributed to final version of the manuscript. AM-E generated all the final figures for the paper.

Declaration of interests

Authors declare no competing interests.

Figure legends

Figure 1. Titan mice, a product of 180 generations of selection, are a giant short-lived mouse strain.

(A) Average weight (g) of 6-wk-old control (blue) and Titan (red) male mice over 180 generations. Generations were composed of roughly 80 pairs of mice, unless stated otherwise (see Methods). Dotted line indicates new mouse housing (see Methods). (B) Representative images of unselected control mice (left) and selected Titan mice (right) at 6 wks. (C) Body length (cm) of 10–11-wk-old Titan mice compared to age-matched control mice. (D) Total fat and lean mass of control (n = 20) and Titan (n = 17) mice. (E) Total percentage of fat in control (n = 20) and Titan (n = 17) mice. (F) Percentage of intra-abdominal fat (n = 10 per group). (G) Comparison of lifespans and mortality rates of Titan and control male mice. (H) After the first four months of life, Titan mice reach 110–115 g, whereas average control animals weigh 45 g. (I). Representative X-ray images of control and Titan mice at 16 wks of age. Control (n = 38) and Titan (n =31) mice were analyzed at 11 wks and at 19–21 wks. ***$P < 0.001$. Error

bars indicate SEMs. Unpaired two-tailed *t*-tests were used to calculate *P*-values.

Figure 2. Titan mice display alterations in fat histology and metabolic homoeostasis.

(A) Representative images of hematoxylin and eosin (H&E)-stained brown adipose tissue (BAT) from control (n = 6) and Titan (n = 5) mice (20x magnification). (B) Representative images of H&E-stained pancreas from control (top) (n = 6) and Titan (n = 6) mice (bottom) (2.5x magnification). (C and D) Leptin levels in control (n = 20) and Titan (n = 18) mice and insulin levels in control (n = 19) and Titan (n = 18) mice. (E) Plasma glucose levels in control (n = 20) and Titan (n = 17) mice. (F and G) FGF-21 levels in control (n = 20) and Titan (n = 18) mice, and alpha-amylase levels in control (n = 20) and Titan (n = 18) mice. ***$P < 0.001$. Error bars indicate SEMs. Unpaired two-tailed *t*-tests were used to calculate *P*-values.

Figure 3. Titan mice show early signs of increased inflammation and impaired metabolism.

(A and B) IL6 levels in control (n = 13) and Titan (n = 17) mice, and TNFα levels in control (n = 20) and Titan (n = 18) mice. (C) Representative images of hematoxylin and eosin (H&E) staining and B-cell immunohistochemistry (IHC) of the thymus of control (left) and Titan (right) mice (2.5x magnification). IHC of thymic medullar nodes revealed that they are composed mainly of B-cells

(CD45R/B220-positive) instead of T-cells (CD3-positive). Images in squares were taken at 10x magnification (n = 4–6 per group). (D and E) Alkaline phosphatase (ALP) and alanine aminotransferase (ALAT) levels in control (n = 20) and Titan mice (n = 18). (F) Red staining of fat in liver of control and Titan mice (n = 4 per group) (G) Bilirubin levels in control (n = 20) and Titan mice (n = 18). (H) Urea levels of control (n = 20) and Titan (n = 18) mice. *$P < 0.05$, **$P < 0.01$ ***$P < 0.001$. Error bars indicate SEMs. Unpaired two-tailed *t*-tests were used to calculate *P*-values.

Figure 4. Liver transcriptome analyses reveal differential expression of genes associated with metabolic pathways in control and Titan mice.

(A) PCA of liver transcriptomes reveals clustering differences between Titan mice and controls. Control mice at 11 wks (younger) and 19–21 wks (older) have similar transcriptomes, while younger and older Titan mice have distinct transcriptomes. (B) Heat map showing significantly altered genes in control and Titan mice at 11 wks and 19–21 wks of age. (C) Pathway enrichment analysis revealed young Titan mice (compared with young control) have altered lipid metabolism, including upregulation of many genes involved in fat and lipid metabolism, whereas various downregulated genes were associated with xenobiotic metabolism. (D) Pathway enrichment analysis revealed that older Titan mice (compared with older control) have increased expression of pathways for regulation of cell to cell adhesion, whereas genes involved in various metabolic pathways such as amino acid metabolism and response to xenobiotics were decreased (n = 5 per group).

Figure 5. Liver proteome analyses reveal differences in metabolic protein levels between control and Titan mice.

(A) Heat map comparing proteomes of 11-wk-old control and Titan mice. (B) Pathway enrichment analysis indicates increased fatty acid synthesis in young Titan mice. In particular, fat utilization and lipid biosynthesis were enhanced. (C) Heat map comparing proteomes of 19–21-wk-old control and Titan mice. (D) Pathway enrichment shows that many upregulated proteins in older Titan mice are linked with lysosome activity, and downregulated proteins are associated with various metabolic pathways such as folate metabolism (n = 6 per group).

Figure 6. Late intervention by switching to energy reduced food (ERF) doubles the pre-mortality plateau phase in Titan mice.

(A) Switching to energy reduced food (ERF) at 12 wks of age (vertical dashed line) increases the time of 10% death and 50% death in Titan mice from 121 to 212 days and 319 to 363 days, respectively. Red/blue shapes re-display data from Figure 1G (n = 102 per group). (B) Switching to ERF at 12 wks results in a persistent average weight loss in Titan siblings. At 21 wks, ERF-fed Titan mice are 10% less heavy than non-ERF siblings (n = 23 per group). (C) Compared to age-matched control Titan mice, ERF-Titan mice have a lower percentage of intra-abdominal fat at 21 weeks (n= 7 per group). (D) Real time PCR comparing gene expression of candidate genes (from Figure 4) of ERF- and control-fed Titan mice siblings at 21 weeks of age (n = 7 per group).

Wilcoxon matched-pairs signed rank test was preformed to calculate P-values. (E) Metabolite analysis in liver following 8 wks on ERF. Malonyl-CoA levels were increased in ERF-fed Titan mice (n= 10 per group). Unpaired two-tailed t-tests were used calculate P-values. (F) Metabolite analysis in liver following 8 wks on ERF. DMG and adenosine were increased and GSSG was decreased in ERF Titan mice (control: n = 9 Titan mice per group; ERF-fed: n = 10 Titan mice per group). *P < 0.05, **P < 0.01. Error bars indicate SEMs.

Methods

Animals and housing conditions

All procedures were performed in accordance to national and international guidelines and approved by our own institutional board (Animal Protection Board from the Leibniz Institute for Farm Animal Biology). At the German Mouse Clinic mice were maintained in IVC cages with water and standard mouse chow according to the directive 2010/63/EU, German laws and GMC housing conditions (www.mouseclinic.de). All tests were approved by the responsible authority of the district government of Upper Bavaria.

The animals were maintained in a specific pathogen-free (SPF) environment with defined hygienic conditions at a temperature of 22.5±0.2°C, at least 40% humidity and a controlled light regime with a 12:12-h light-dark cycle. The mice were kept in Polysulfon-cages of 365 x 207 x 140 mm (H-Temp PSU, Type II L, Eurostandard, Tecniplast, Germany) and had free access to pellet concentrate and water. A standard breeding diet (SD) with 22% crude protein,

34% starch, 5% sugar, 4.5% crude fat, 3.9% crude fiber and 51.2% N free extracts (ssniff® M-Z autoclavable, Soest, Germany) were fed ad libitum.

For the energy reduced survival experiment the mice were fed with a mouse maintenance energy reduced diet (ERF) characterized by a low energy density and high fiber contents (15% crude protein, 21% starch, 5% sugar, 3.1% crude fat, 14.2% crude fiber and 48.8% N free extracts (ssniff® M-H autoclavable, Soest, Germany). Feeding the energy reduced diet started with an age of 12 wks.

During the survival experiments all included males were observed daily for their health condition. If physical impairments were detected which would cause considerable suffering or substantial pain to the animals they were sacrificed and such incidents were documented accordingly.

Origins of the growth selected strain and the control strain.

We used mice of an unselected strain (FZTDU) as control and a strain selected for high body mass at day 42 of age (DU6/Titan), both bred at the Leibniz Institute of Farm Animal Biology (FBN), Dummerstorf, Germany.

The initial population of mice was created in 1969/1970 by crossing four outbred (NMRI orig., Han/NMRI, CFW, CF1) and four inbred (CBA/Bln, AB/Bln, C57BL/Bln, XVII/Bln) populations (Schüler, 1985). Mice of the control line FZTDU used in this experiment were mated randomly over about 192 generations with a population size of 100 to 200 mating pairs per generation,

respectively. Four generations of the control line are generated yearly using a rotation procedure of Poiley (1960) to avoid inbreeding (Poiley, 1960).

The growth selection started in 1975 thus creating the Dummerstorf growth line DU6 (Titan) by selection for high body mass by sib selection (Bünger et al., 2001) in a conventional environment. In every generation, 80 pair mating were made at an age of 63 ± 3d (Bünger et al., 1998). Selection procedure as described above was maintained for 153 generations. Only seven males and seven females of the DU6 line belonging to generation 153 and 154, respectively, were used as new founder animals after embryo transfer in a new built animal facility. Additionally, the health status has been changed after 2011 when the mouse lines were transferred into a new animal facility with specific pathogen free environment conditions. Over the entire term of the following five generations the new breeding population of at least 60 pairs of Titan DU6 mice were established taking care of an equal distribution of all genes of the 14 founder animals. In opposition to the former sib selection in generation number 161, breeding value estimation started introducing a two trait BLUP (**B**est Linear **U**nbiased **P**rediction) animal model for male and female body mass. The raising inbreeding coefficient in the selection line was then controlled by the method ‘Optimal Genetic Contributions to the Next Generations’ of Meuwissen (Meuwissen, 1997).

Histology, plasma, DEXA – GMC

Phenotypic screening

At the GMC, a cohort of 20 male DU6/Titan mice and 20 male controls (FZTDU) at the age of 9-11 wks and a cohort of 20 male Du6/Titan mice (Figure S3) and 20 male controls at the age of 19-21 wks were subjected to an extensive phenotypic screening at the German Mouse Clinic, including standardized phenotyping in the areas of energy metabolism, clinical chemistry, pathology (Gailus-Durner et al., 2005) (see also www.mouseclinic.de). The phenotypic tests were part of the GMC screen and were performed according to standardized protocols as described before (Fuchs et al., 2011; Rathkolb et al., 2013) (Rozman et al., 2015).

Variations in protocols are specified. Dependent of the test performed, animal number may vary, and is indicated in the figure/table.

The determination of the IL6, TNFα, Insulin, leptin and FGF-21 was performed with a combined electrochemiluminescence multiplexed assay system (Meso Scale Discovery, MSD, Rockville, MD USA).

X-ray imaging was performed in an UltraFocus DXA system (Faxitron Bioptics, LLC) with automatic exposure control.

For histopathological analyses, hematoxylin and eosin (H&E) staining was performed on formalin-fixed paraffin-embedded sections (3 µm).

A macroscopic examination was performed in combination with histopathological analyses using hematoxylin and eosin (H&E) staining on formalin-fixed paraffin-embedded sections (3 µm) of tissues of 29 organs as

described in www.mouseclinic.de/screens/pathology. Immunohistochemistry was carried out in a Leica Bond III (Leica Biosystems) automatic strainer. Heat-induced antigen retrieval was performed with citrate buffer (pH 6) for 30 minutes (AR9961; Bond TM Epitope Retrieval Solution; Leica Bio systems) in 2-µm-thick sections. For the identification of specific cells in the thymus antibodies against CD3 (Clone SP7; ZYT-RBG024; Zytomed systems) and CD45R/B220 (Clone RA3-6B2; 550286; BD Pharmingen) were employed and the staining was detected with DAB chromogen. The slides were scanned using a Hamamatsu NanoZoomer 2.0HT digital scanner and analysed by two independent pathologists using NDP.view2 software (Hamamatsu Photonics).

RNAseq

RNA extraction, quality control and library preparation:

50 mg of tissues were homogenized in Trizol (Thermo Fisher; cat. no. 15596026) and processed according to the manufacturer's instructions. RNA concentration and $A_{260/280}$ ratio was measured with NanoDrop, followed by Bioanalyzer using RNA pico assay kit using manufacturer's protocol. rRNA depletion was performed using NEBNext rRNA Depletion Kit (Human/Mouse/Rat) [NEB #E6310] and library preparation for RNA-sequencing was performed using NEBNext Ultra II Directional RNA Library Prep Kit for Illumina [NEB #E7760] following manufacturer's protocol.

RNA-seq data analysis:

Read mapping of mouse tissue samples to the mouse genome (GRCm38) and counting of reads mapped to genes were performed using STAR v2.5.3a (Dobin and Gingeras, 2015) using parameters --quantMode GeneCounts and providing annotation –sjdbGTFfile Mus_musculus.GRCm38.97.gtf. Aligned reads were filtered for unmapped, multimapped and ambiguous reads. Reads from histones and Y chromosome were also removed. Reads were also filtered if they have low read counts in at least 2 samples. Differential expression analysis was carried out using DESeq2 v1.24.0 (Love et al., 2014) at an adjusted p-value cut-off of 0.05. GO term analysis was performed using ClusterProfiler v3.12.0 (Yu et al., 2012) at a FDR of 0.05 using Benjamini-Hochberg procedure and with a log fold change cut-off of 0.5. GO terms containing at least a minimum of 10 genes were considered.

All the plots generated for RNA sequencing data was obtained using ggplot2 v3.2.1 (H. Wickham. ggplot2: Elegant Graphics for Data Analysis. Springer-Verlag New York, 2016) unless otherwise stated. For heatmaps and Venn diagram for RNA sequencing and proteomics data, pheatmap v1.0.12 (Kolde, R. (2013). pheatmap: Pretty Heatmaps. R package version 0.7.7. http://CRAN.R-project.org/package=pheatmap) and VennDiagram v1.6.20(H. Chen and Boutros, 2011) were used respectively with genes (or proteins) passing the adjusted p-value significance of 0.05.

Proteomics

Liver proteome and acetylome sample preparation

The proteome and acetylome protocol was adopted from (Gaucher et al., 2019; Peleg et al., 2016a) with the following modifications. 200 mg of frozen mice liver was homogenized in 500 µl lysis buffer [50 mM Tris-HCl pH 7.5, 500 mM NaCl, 1 ml EDTA, 0.1% NP-40 and 20% glycerol, 15 mM sodium butyrate, 60 mM of sirtinol and one protease inhibitor tablet (Roche)] and then added with 200 µl 6 M urea/2 M thiourea and 900µl lysis buffer. To reduce disulfide bonds samples were treated with 1 mM DTT for 45 min at 4°C, followed by a treatment with 550 mM IAA for 30min at 4°C in the dark. 1 M ammonium bicarbonate (Ambic) was added to the samples to get a final concentration of 1 M urea. The proteins were digested for 5h with Lys-C (Wako) at room temperature and overnight with trypsin (Worthington). Samples were acidified and diluted with TFA to a final concentration of 1% TFA before loaded on the Sep-Pak Light C18 cartridges (Waters). Columns were washed with 0.1% TFA and eluted with 60% acetonitrile (ACN)/0.25% TFA. The elutes were speed vacuumed until they were dry. The pellets were re-dissolved with IP buffer [50 mM Hepes pH 8.0 and 50 mM NaCl] and the protein concentration was measured by Nanodrop. For the proteome, total peptide amount of ca. 4 µg per samples were taken prior to the acetylation enrichment and were desalted as previously described (REF). The dried pellets were reconstituted in 16 µl MS injection buffer (2% ACN, 0.1% FA) and final peptide concentration were determined using Nanodrop.

For acetylome analysis equal concentrations of peptides were incubated with 45 µl anti-acetyllysine antibody (ImmuneChem) overnight at 4°C. Beads were washed 4x with PBS/Tween 0.1% and then 4x with PBS. Acetylated peptides were eluted from beads with 125 µl 0.1% TFA, diluted with 80 µl 0.1% TFA, desalted using self-packed StageTips (three disks, ø 1.5mm, C18 material, 3M Empore), dried down, reconstituted in 12 µl MS injection buffer (2% ACN, 0.1% FA) and analysed by mass spectrometry.

LC-MS/MS data acquisition

LC-MS/MS measurements were performed on an Ultimate 3000 RSLCnano system coupled to a Q-Exactive HF-X mass spectrometer (Thermo Fisher Scientific). For full proteome analyses ~0.25 µg of peptides were delivered to a trap column (ReproSil-pur C18-AQ, 5 µm, Dr. Maisch, 20 mm × 75 µm, self-packed) at a flow rate of 5 µL/min in 100% solvent A (0.1% formic acid in HPLC grade water). For acetylome analyses the complete elute after acetylome-enrichment and desalting was injected. For each MS-analysis, peptides were delivered to a trap column (ReproSil-pur C18-AQ, 5 µm, Dr. Maisch, 20 mm × 75 µm, self-packed) at a flow rate of 5 µL/min in 0.1% formic acid in HPLC grade water. After 10 minutes of loading, peptides were transferred to an analytical column (ReproSil Gold C18-AQ, 3 µm, Dr. Maisch, 450 mm × 75 µm, self-packed) and separated using a 110 min gradient from 4% to 32% of solvent B (0.1% formic acid in acetonitrile and 5% (v/v) DMSO) at 300 nL/min flow rate. Both nanoLC solvents (solvent A = 0.1% formic acid in HPLC grade water and 5% (v/v) DMSO) contained 5% DMSO to boost MS intensity.

The Q-Exactive HF-X mass spectrometer was operated in data dependent acquisition (DDA) and positive ionization mode. MS1 spectra (360–1300 m/z) were recorded at a resolution of 60,000 using an automatic gain control (AGC) target value of 3e6 and maximum injection time (maxIT) of 45 msec. Up to 18 peptide precursors were selected for fragmentation in case of the full proteome analyses, while only up to 12 peptide precursor were selected for the acetylome analyses. Only precursors with charge state 2 to 6 were selected and dynamic exclusion of 30 sec was enabled. Peptide fragmentation was performed using higher energy collision induced dissociation (HCD) and a normalized collision energy (NCE) of 26%. The precursor isolation window width was set to 1.3 m/z. MS2 Resolution was 15.000 with an automatic gain control (AGC) target value of 1e5 and maximum injection time (maxIT) of 25 msec (full proteome) or 100 msec (acetylome).

Database searching

Peptide identification and quantification was performed using MaxQuant (version 1.6.3.4) with its built-in search engine Andromeda (Cox et al., 2011; Tyanova et al., 2016). MS2 spectra were searched against the Uniprot mus musculus proteome database (UP000000589, 54,208 protein entries, downloaded 22.3.2019) supplemented with common contaminants (built-in option in MaxQuant). Trypsin/P was specified as proteolytic enzyme. Precursor tolerance was set to 4.5 ppm, and fragment ion tolerance to 20 ppm. Results were adjusted to 1 % false discovery rate (FDR) on peptide spectrum match (PSM) level and protein level employing a target-decoy approach using

reversed protein sequences. The minimal peptide length was defined as 7 amino acids, the “match-between-run” function was disabled. For full proteome analyses carbamidomethylated cysteine was set as fixed modification and oxidation of methionine and N-terminal protein acetylation as variable modifications. For acetylome analyses carbamidomethylated cysteine was set as fixed modification and oxidation of methionine, N-terminal protein acetylation and acetylation of lysines as variable modifications.

Statistical proteomic analysis

Six biological replicates were measured in young and old Titan as well as young and old control mice. Intensities of acetylated peptides were computed with MaxQuant and used to represent acetylated peptide abundances. Protein abundances were calculated using the LFQ algorithm from MaxQuant (Cox et al., 2014). Before further downstream analyses, protein LFQ values and acetylated peptide intensities were logarithm (base 10) transformed. The median intensity of acetylated peptides of every sample was aligned so that the overall acetylated peptides intensities are comparable across samples. Next, Limma (Ritchie et al., 2015) was used to identify the differentially expressed proteins and acetylated peptides between young control vs young Titan; young control vs old control; young Titan vs old Titan and old control vs old Titan. The resulted p-values were adjusted by the Benjamini-Hochberg algorithm (Benjamini and Hochberg, 1995) to control the false discovery rate (FDR). The differential analyses were performed on proteins/acetylated peptides that are identified in at least four out of six biological replicate samples in both groups under comparison.

Gene set annotations were downloaded from MSigDB (Liberzon et al., 2015), including the Gene Ontology annotation (C5 category) and pathway annotation (C2 category). The gene IDs of differentially expressed proteins/acetylated peptides were mapped to the gene set annotations. The significance of over-representation was evaluated using fisher's exact test.

Total RNA extraction for Real Time PCR

RNA extraction was prepared from 50mg deep frozen liver tissue. The tissue was homogenized in 1ml TRItidy G™ via pestle and incubated at room temperature for 5 minutes. After addition of 200µl chloroform the sample was mixed 15 seconds with the Vortex and again incubated for 2 minutes at room temperature with a following centrifugation step at 12000x g, 4°C for 15 minutes. The aqueous phase was filled in a new vial and mixed with 500µl -20°C isopropanol and incubated 10 minutes at -20°C. The samples were then centrifuged at 8000x g, 4°C for 10 minutes and the supernatant was discarded. 2 wash steps with 1ml -20°C cold 70% ethanol were followed. The clean pellet was air-dried and dissolved in 100µl nuclease free water. RNA concentration was measured with NanoDrop 2000.

Quantitative real-time PCR

800ng RNA was taken for cDNA synthesis. The cDNA was generated using the SensiFAST™cDNA Synthesis Kit (Bioline). For the PCR reaction was used the SensiFAST™SYBR® No-Rox Kit (Bioline). The cDNA concentration in all

reactions was 1,25ng except mTOR (here 2,5ng) and the primer concentration was 4pmol. RT-PCR was performed using the Roche Lightcycler 96. The annealing temperature was 60°C. The RT-PCR results were normalized to the levels of beta actin. Primers are listed in Table**.** PCR products were cleaned up using the High Pure PCR Product Purification Kit (Roche) and sequenced by LGC Genomics GmbH. Each sample was measured using two technical replicates.

Staining of triglycerides in liver tissues

Liver tissue samples embedded in Tissue Tek (Weckert, Kitzingen, Germany) were cryosectioned (5 µm thick) using a Leica CM3050 S (Leica, Bensheim, Germany) cryostat microtome. After fixation in 4% paraformaldehyde / PBS for 30 min at RT, the slides were stained in RedOil solution (1 mg/ml RedOil (#A12989, Alfa Aesar, Karlsruhe, Germany) in 60% Isopropanol) for 10 min and then washed three times in distilled water. The stained slides were covered with Aquatex (Roth, Germany) and dried overnight. The staining of the triglycerides was visualized with a Nikon Microphot-Fxa microscope (Nikon Instruments Europe B.V., The Netherlands) and an image analysis system (Nikon Digital Sight, DS-L2).

Metabolite profiling of the liver

Metabolomic profiling was conducted using ion pairing reversed phase liquid chromatography- high resolution mass spectrometry (LC-HRMS) modified from previous methods for polar analytes (Guo et al., 2016) and nucleotides

(Kuskovsky et al., 2019). Samples were spiked with a stable isotope mix containing $^{13}C_3$-Sodium Pyruvate, $^{13}C_3$-Lactate, $^{13}C_4$-Fumaric Acid, $^{13}C_4$-Succinic acid, $^{13}C_4{}^{15}N_1$-Aspartic Acid, $^{13}C_6$-Citric Acid, $^{13}C_6$-Glucose-6-phosphate, $^{13}C_2$-AcetylCoA, $^{13}C_5$-D-α-Hydroxyglutaric acid, $^{13}C_5{}^{15}N_2$-Glutamine from Sigma-Aldrich or Cambridge Isotope Laboratories. 1 mL of Optima LC-MS grade 80:20 methanol:water prechilled to -80˚C was then added to each sample, followed by a 30 second vortex mixing, 15 second pulse sonication with a probe tip sonicator then samples were returned to the -80 ˚C freezer for 30 min. Insoluble debris was precipitated by centrifugation for 10 min, 17,000 x g at 4˚C. Supernatant was evaporated to dryness under nitrogen, resuspended in 100 µL 5% 5-sulfosaliclyic acid in water, and 5 µL was injected for analysis. LC-HRMS was conducted on an Ultimate 3000 UHPLC equipped with a refrigerated autosampler (at 6 °C) and a column heater (at 55 °C) with a HSS C18 column (2.1 × 100 mm i.d., 3.5 µm; Waters, Milford, MA) used for separations. Solvent A was 5 mM DIPEA and 200 mM HFIP and solvent B was methanol with 5 mM DIPEA 200 mM HFIP. The gradient was as follows: 100 % A for 3 min at 0.18 mL/min, 100 % A at 6 min with 0.2 mL/min, 98 % A at 8 min with 0.2 mL/min, 86 % A at 12 min with 0.2 mL/min, 40 % A at 16 min and 1 % A at 17.9 min-18.5 min with 0.3 mL/min then increased to 0.4 mL/min until 20 min. Flow was ramped down to 0.18 mL/min back to 100 % A over a 5 min re-equilibration. For MS analysis, the UHPLC was coupled to a Q Exactive HF mass spectrometer (Thermo Scientific, San Jose, CA, USA) equipped with a HESI II source operating in negative mode. The operating conditions were as follows: spray voltage 4000 V; vaporizer temperature 200 °C; capillary temperature 350 °C; S-lens 60; in-source CID 1.0 eV, resolution 60,000. The

sheath gas (nitrogen) and auxiliary gas (nitrogen) pressures were 45 and 10 (arbitrary units), respectively. Single ion monitoring (SIM) windows were acquired around the $[M-H]^-$ of each analyte with a 20 *m/z* isolation window, 4 *m/z* isolation window offset, $1e^6$ ACG target and 80 ms IT, alternating in a Full MS scan from 70-950 *m/z* with 1e6 ACG, and 100 ms IT. Data was analyzed in XCalibur v4.0 and/or Tracefinder v4.1 (Thermo) using a 5 ppm window for integration of the peak area of all analytes and internal standards used for normalization.

Statistics and graphing

Unless stated otherwise in the RNA-seq and proteomics experimental method, statistics and graphing was conducted on GraphPad Prism 8. For real-time PCR experiments, Wilcoxon matched-pairs signed rank test was preformed. Otherwise, unpaired two-tailed *t*-tests were used for calculating the *P*-values

Importantly, according to the GMC analysis outline, no FDR rate was performed in analyzing the GMC data set.

Data availability

All LC-MS/MS data files and MaxQuant output files have been deposited to the ProteomeXchange Consortium (http://proteomecentral.proteomexchange.org) via the PRIDE partner repository with the dataset identifier PXDXXX. All RNAseq data have been deposited to GEO.

Supplementary figures

Figure S1. Whitening of brown adipose tissue (BAT) in Titan mice

Hematoxylin and eosin (H&E) staining images of BAT from 4 months old control and Titan mice are shown (20x magnification; n = 4 per group). Representative pictures are shown in Figure 2A.

Figure S2. Pancreatic lipomatosis was observed in Titan mice.

H&E staining images of the pancreas from 4 months old control and Titan mice are shown (2.5x magnification; n = 4 per group). Higher magnification pictures were taken at 20x. Representative pictures are shown in Figure 2B.

Figure S3. Plasma analysis comparing control and Titan mice after fasting.

(A-D) Younger Titan mice show higher levels of triglycerides and both non HDL and HDL cholesterol (n= 20 control vs 19 Titan). *$P < 0.05$, **$P < 0.01$ ***$P < 0.001$. Error bars indicate SEMs. Unpaired two-tailed *t*-tests were used to calculate *P*-values.

Figure S4. Titan mice show nodular thymic medullary hyperplasia.

H&E staining images of the thymus from 4 months old control and Titan mice are shown (2.5x magnification; n = 4 per group). Higher magnification pictures were taken at 20x. Black arrows indicate normal medulla and the white ones hyperplastic medulla. Representative pictures are shown in Figure 3C.

Figure S5. Hyperplastic nodules in the thymic medulla of Titan mice are mainly composed of B cells.

CD45R/B220 IHC shows a considerably increased presence of B cells in the medulla of the thymus in Titan mice (10x magnification; n = 4 per group).

Figure S6. Liver histology of control vs Titan mice

Shown are H&E-stained images of the liver from 4 months old control and Titan mice. In addition, 6 months old Titan liver pictures are displayed (10x magnification; n = 4 per group). No obvious histological alterations were observed between the groups.

Figure S7. Iron levels and related binding capacity is altered in Titan mice.

Titan mice have an excess of iron in plasma, together with high transferrin saturation, low UIBC and low TIBC compared to control mice. n = 20 control vs 18 Titan for iron, N = 20 control vs 12 Titan for UIBC (unsaturated iron binding capacity), TIBC (Total Iron Binding Capacity) and calc. (Calculated) transferrin saturation. $^{**}P < 0.01$ $^{***}P < 0.001$. Error bars indicate the SEM in all the graphs. Unpaired two-tailed *t*-tests were used for calculating the *P*-values.

Figure S8. Kidney histology of control vs Titan mice

Kidney tissue comparison of 4 old months control vs 4- and 6-months old Titan mice. Arrows indicate basophilic tubules as well as tubular casts, which are seen in the kidneys of several of the Titan mice.

Figure S9. Plasma electrolytes analysis show increased levels of calcium, potassium and inorganic phosphate.

(A-C) Titan mice show higher levels of plasma calcium, potassium and inorganic phosphate (n = 20 control vs 18 Titan). ***$P < 0.001$. Error bars indicate the SEM in all the graphs. Unpaired two-tailed *t*-tests were used for calculating the *P*-values.

Figure S10. Increased cardiac fibrosis was found in Titan mice

H&E and Sirius Red staining of the heart from 4 months old control and Titan mice are shown (0.45x magnification). Sirius Red staining allows a better visualization of fibrotic tissue. Higher magnification pictures from rectangles were taken at 10x. Increased cardiac fibrosis was found in 3/6 young and 5/6 older Titan mice.

Figure S11. Transcriptome changes in the Liver of younger vs older Titan mice

(A) Heat map showing significantly altered genes between younger control vs younger Titan mice. (B) Heat maps showing significantly altered genes between young and older Titan mice. (C) Pathway enrichment analysis of (B) revealed an increase in insulin pathway and glucose homeostasis and decrease in various metabolic processes including fatty acid metabolism. (D) Heat map showing significantly altered genes between older control vs older Titan mice ‘younger’ (11 wks) and ‘older’ (19-21 wks) mice. n=5 per group.

Figure S12. Commonly altered liver genes/proteins between control and Titan mice

(A-D) Venn diagrams showing commonly regulated genes/proteins in the liver transcriptome/proteome. (A) Upregulated genes vs upregulated proteins in younger Titan mice compared to younger control mice. (B) Down regulated genes vs down regulated proteins in younger Titan mice compared to younger control mice. (C) Upregulated genes vs upregulated proteins in older Titan mice compared to older control mice. (D) Down regulated genes vs down regulated proteins in older Titan mice compared to older control mice. N=6 per group.

Figure S13. Liver acetylome analyses revealed hypo-acetylation in younger Titan mice

(A) Heat map comparing the acetylome between younger controls to Titan. 17 upregulated and 117 downregulated proteins in young Titan. (B) Pathway enrichment show increased protein acetylation in several proteins in lipid metabolism in Titan mice. (C) Pathway enrichment show decreased protein acetylation in Titan mice in various mitochondrial proteins, translation process and several metabolic pathways including glycine and serine metabolism. n=6 per group.

Figure S14. Targeted metabolite analysis of intra-abdominal fat comparing control food vs ERF Titan mice at 21 weeks of age

Metabolite profiling of intraabdominal fat following ERF intervention in Titan mice. Similarly to liver, energy reduced fed Titan mice display higher levels of DMG and adenosine compared to control Titan. N= 9 per group

References

Agrawal, S., Zaritsky, J.J., Fornoni, A., Smoyer, W.E., 2017. Dyslipidaemia in nephrotic syndrome: mechanisms and treatment. Nat Rev Nephrol 14, 70. doi:10.1038/nrneph.2017.175

Altintas, O., Park, S., Lee, S.-J.V., 2016. The role of insulin/IGF-1 signaling in the longevity of model invertebrates, C. elegans and D. melanogaster. BMB Rep 49, 81–92. doi:10.5483/bmbrep.2016.49.2.261

Alwaili, K., Bailey, D., Awan, Z., Bailey, S.D., Ruel, I., Hafiane, A., Krimbou, L., Laboissiere, S., Genest, J., 2012. The HDL proteome in acute coronary syndromes shifts to an inflammatory profile. Biochim. Biophys. Acta 1821, 405–415. doi:10.1016/j.bbalip.2011.07.013

Assmann, G., Gotto, A.M., 2004. HDL cholesterol and protective factors in atherosclerosis. Circulation 109, III8–14. doi:10.1161/01.CIR.0000131512.50667.46

Asztalos, B.F., Tani, M., Schaefer, E.J., 2011. Metabolic and functional relevance of HDL subspecies. Curr. Opin. Lipidol. 22, 176–185. doi:10.1097/MOL.0b013e3283468061

Ayoub, H.M., McDonald, M.R., Sullivan, J.A., Tsao, R., Meckling, K.A., 2018. Proteomic Profiles of Adipose and Liver Tissues from an Animal Model of Metabolic Syndrome Fed Purple Vegetables. Nutrients 10. doi:10.3390/nu10040456

Baker, D.J., Childs, B.G., Durik, M., Wijers, M.E., Sieben, C.J., Zhong, J., Saltness, R.A., Jeganathan, K.B., Verzosa, G.C., Pezeshki, A., Khazaie, K., Miller, J.D., van Deursen, J.M., 2016. Naturally occurring p16(Ink4a)-

positive cells shorten healthy lifespan. Nature 530, 184–189. doi:10.1038/nature16932

Bartke, A., 2003. Can growth hormone (GH) accelerate aging? Evidence from GH-transgenic mice. Neuroendocrinology 78, 210–216. doi:10.1159/000073704

Benjamini, Y., Hochberg, Y., 1995. Controlling the False Discovery Rate: A Practical and Powerful Approach to Multiple Testing

. Journal of the Royal Statistical Society 57, 289–300.

Blutke, A., Schneider, M.R., Wolf, E., Wanke, R., 2016. Growth hormone (GH)-transgenic insulin-like growth factor 1 (IGF1)-deficient mice allow dissociation of excess GH and IGF1 effects on glomerular and tubular growth. Physiol Rep 4. doi:10.14814/phy2.12709

Bonomini, F., Rodella, L.F., Rezzani, R., 2015. Metabolic syndrome, aging and involvement of oxidative stress. Aging Dis 6, 109–120. doi:10.14336/AD.2014.0305

Brayton, C.F., Treuting, P.M., Ward, J.M., 2012. Pathobiology of aging mice and GEM: background strains and experimental design. Vet. Pathol. 49, 85–105. doi:10.1177/0300985811430696

Brüünsgaard, H., Pedersen, B.K., 2003. Age-related inflammatory cytokines and disease. Immunol Allergy Clin North Am 23, 15–39. doi:10.1016/s0889-8561(02)00056-5

Bünger, L., Laidlaw, A., Bulfield, G., Eisen, E.J., Medrano, J.F., Bradford, G.E., Pirchner, F., Renne, U., Schlote, W., Hill, W.G., 2001. Inbred lines of mice derived from long-term growth selected lines: unique resources for mapping

growth genes. Mamm. Genome 12, 678–686. doi:10.1007/s00335001-3018-6

Bünger, L., Renne, U., Dietl, G., Kuhla, S., 1998. Long-term selection for protein amount over 70 generations in mice. Genet. Res. 72, 93–109. doi:10.1017/s0016672398003401

Calado, R.T., Dumitriu, B., 2013. Telomere dynamics in mice and humans. Semin. Hematol. 50, 165–174. doi:10.1053/j.seminhematol.2013.03.030

Candore, G., Caruso, C., Jirillo, E., Magrone, T., Vasto, S., 2010. Low grade inflammation as a common pathogenetic denominator in age-related diseases: novel drug targets for anti-ageing strategies and successful ageing achievement. Curr. Pharm. Des. 16, 584–596. doi:10.2174/138161210790883868

Catanzaro, R., Cuffari, B., Italia, A., Marotta, F., 2016. Exploring the metabolic syndrome: Nonalcoholic fatty pancreas disease. World J. Gastroenterol. 22, 7660–7675. doi:10.3748/wjg.v22.i34.7660

Chen, H., Boutros, P.C., 2011. VennDiagram: a package for the generation of highly-customizable Venn and Euler diagrams in R. BMC Bioinformatics 12, 35. doi:10.1186/1471-2105-12-35

Chen, L.Y., Chang, S.D., Sreenivasan, G.M., Tsang, P.W., Broady, R.C., Li, C.H., Zypchen, L.N., 2011. Dysmetabolic hyperferritinemia is associated with normal transferrin saturation, mild hepatic iron overload, and elevated hepcidin. Ann. Hematol. 90, 139–143. doi:10.1007/s00277-010-1050-x

Cheng, X., Zhu, B., Jiang, F., Fan, H., 2011. Serum FGF-21 levels in type 2 diabetic patients. Endocr. Res. 36, 142–148. doi:10.3109/07435800.2011.558550

Choi, W.-S., Lee, G., Song, W.-H., Koh, J.-T., Yang, J., Kwak, J.-S., Kim, H.-E., Kim, S.K., Son, Y.-O., Nam, H., Jin, I., Park, Z.-Y., Kim, J., Park, I.Y., Hong, J.-I., Kim, H.A., Chun, C.-H., Ryu, J.-H., Chun, J.-S., 2019. The CH25H-CYP7B1-RORα axis of cholesterol metabolism regulates osteoarthritis. Nature 566, 254–258. doi:10.1038/s41586-019-0920-1

Chou, M.W., Kong, J., Chung, K.T., Hart, R.W., 1993. Effect of caloric restriction on the metabolic activation of xenobiotics. Mutat. Res. 295, 223–235. doi:10.1016/0921-8734(93)90022-u

Choudhary, C., Weinert, B.T., Nishida, Y., Verdin, E., Mann, M., 2014. The growing landscape of lysine acetylation links metabolism and cell signalling. Nat. Rev. Mol. Cell Biol. 15, 536–550. doi:10.1038/nrm3841

Cox, J., Hein, M.Y., Luber, C.A., Paron, I., Nagaraj, N., Mann, M., 2014. Accurate proteome-wide label-free quantification by delayed normalization and maximal peptide ratio extraction, termed MaxLFQ. Mol. Cell Proteomics 13, 2513–2526. doi:10.1074/mcp.M113.031591

Cox, J., Neuhauser, N., Michalski, A., Scheltema, R.A., Olsen, J.V., Mann, M., 2011. Andromeda: a peptide search engine integrated into the MaxQuant environment. J. Proteome Res. 10, 1794–1805. doi:10.1021/pr101065j

Crimmins, E.M., 2015. Lifespan and Healthspan: Past, Present, and Promise. Gerontologist 55, 901–911. doi:10.1093/geront/gnv130

Crocco, P., Montesanto, A., Dato, S., Geracitano, S., Iannone, F., Passarino, G., Rose, G., 2019. Inter-Individual Variability in Xenobiotic-Metabolizing Enzymes: Implications for Human Aging and Longevity. Genes (Basel) 10. doi:10.3390/genes10050403

Di Francesco, A., Di Germanio, C., Bernier, M., de Cabo, R., 2018. A time to fast. Science 362, 770–775. doi:10.1126/science.aau2095

Ding, J., Berryman, D.E., Kopchick, J.J., 2011. Plasma proteomic profiles of bovine growth hormone transgenic mice as they age. Transgenic Res. 20, 1305–1320. doi:10.1007/s11248-011-9499-5

Dobin, A., Gingeras, T.R., 2015. Mapping RNA-seq Reads with STAR. Curr Protoc Bioinformatics 51, 11.14.1–11.14.19. doi:10.1002/0471250953.bi1114s51

Eller, P., Hochegger, K., Wehinger, A., Tancevski, I., Schgoer, W., Ritsch, A., Patsch, J.R., 2006. Hepatic ENPP1 expression is induced in diabetic rabbits. Mamm. Genome 17, 886–891. doi:10.1007/s00335-006-0028-4

Folgueras, A.R., Freitas-Rodríguez, S., Velasco, G., López-Otín, C., 2018. Mouse Models to Disentangle the Hallmarks of Human Aging. Circ. Res. 123, 905–924. doi:10.1161/CIRCRESAHA.118.312204

Fontana, L., Partridge, L., 2015. Promoting health and longevity through diet: from model organisms to humans. Cell 161, 106–118. doi:10.1016/j.cell.2015.02.020

Franceschi, C., Campisi, J., 2014. Chronic inflammation (inflammaging) and its potential contribution to age-associated diseases. J. Gerontol. A Biol. Sci. Med. Sci. 69 Suppl 1, S4–9. doi:10.1093/gerona/glu057

Frei, B., Stocker, R., Ames, B.N., 1988. Antioxidant defenses and lipid peroxidation in human blood plasma. Proc. Natl. Acad. Sci. U.S.A. 85, 9748–9752. doi:10.1073/pnas.85.24.9748

Fuchs, H., Gailus-Durner, V., Adler, T., Aguilar-Pimentel, J.A., Becker, L., Calzada-Wack, J., Da Silva-Buttkus, P., Neff, F., Götz, A., Hans, W., Hölter,

S.M., Horsch, M., Kastenmüller, G., Kemter, E., Lengger, C., Maier, H., Matloka, M., Möller, G., Naton, B., Prehn, C., Puk, O., Racz, I., Rathkolb, B., Römisch-Margl, W., Rozman, J., Wang-Sattler, R., Schrewe, A., Stöger, C., Tost, M., Adamski, J., Aigner, B., Beckers, J., Behrendt, H., Busch, D.H., Esposito, I., Graw, J., Illig, T., Ivandic, B., Klingenspor, M., Klopstock, T., Kremmer, E., Mempel, M., Neschen, S., Ollert, M., Schulz, H., Suhre, K., Wolf, E., Wurst, W., Zimmer, A., Hrabe de Angelis, M., 2011. Mouse phenotyping. Methods 53, 120–135. doi:10.1016/j.ymeth.2010.08.006

Fuentes, M., Santander, N., Cortés, V., 2018. Insulin increases cholesterol uptake, lipid droplet content, and apolipoprotein B secretion in CaCo-2 cells by upregulating SR-BI via a PI3K, AKT, and mTOR-dependent pathway. J. Cell. Biochem. doi:10.1002/jcb.27410

Fulop, T., Le Page, A., Fortin, C., Witkowski, J.M., Dupuis, G., Larbi, A., 2014. Cellular signaling in the aging immune system. Curr. Opin. Immunol. 29, 105–111. doi:10.1016/j.coi.2014.05.007

Gailus-Durner, V., Fuchs, H., Becker, L., Bolle, I., Brielmeier, M., Calzada-Wack, J., Elvert, R., Ehrhardt, N., Dalke, C., Franz, T.J., Grundner-Culemann, E., Hammelbacher, S., Hölter, S.M., Hölzlwimmer, G., Horsch, M., Javaheri, A., Kalaydjiev, S.V., Klempt, M., Kling, E., Kunder, S., Lengger, C., Lisse, T., Mijalski, T., Naton, B., Pedersen, V., Prehn, C., Przemeck, G., Racz, I., Reinhard, C., Reitmeir, P., Schneider, I., Schrewe, A., Steinkamp, R., Zybill, C., Adamski, J., Beckers, J., Behrendt, H., Favor, J., Graw, J., Heldmaier, G., Höfler, H., Ivandic, B., Katus, H., Kirchhof, P., Klingenspor, M., Klopstock, T., Lengeling, A., Müller, W., Ohl, F., Ollert, M., Quintanilla-Martinez, L., Schmidt, J., Schulz, H., Wolf, E., Wurst, W.,

Zimmer, A., Busch, D.H., de Angelis, M.H., 2005. Introducing the German Mouse Clinic: open access platform for standardized phenotyping. Nat. Methods 2, 403–404. doi:10.1038/nmeth0605-403

Gaucher, J., Kinouchi, K., Ceglia, N., Montellier, E., Peleg, S., Greco, C.M., Schmidt, A., Forne, I., Masri, S., Baldi, P., Imhof, A., Sassone-Corsi, P., 2019. Distinct metabolic adaptation of liver circadian pathways to acute and chronic patterns of alcohol intake. Proc. Natl. Acad. Sci. U.S.A. 116, 25250–25259. doi:10.1073/pnas.1911189116

Gimbrone, M.A., García-Cardeña, G., 2016. Endothelial Cell Dysfunction and the Pathobiology of Atherosclerosis. Circ. Res. 118, 620–636. doi:10.1161/CIRCRESAHA.115.306301

Gowda, S., Desai, P.B., Hull, V.V., Math, A.A.K., Vernekar, S.N., Kulkarni, S.S., 2009. A review on laboratory liver function tests. Pan Afr Med J 3, 17.

Greer, E.L., Brunet, A., 2009. Different dietary restriction regimens extend lifespan by both independent and overlapping genetic pathways in C. elegans. Aging Cell 8, 113–127. doi:10.1111/j.1474-9726.2009.00459.x

Grundy, S.M., Cleeman, J.I., Daniels, S.R., Donato, K.A., Eckel, R.H., Franklin, B.A., Gordon, D.J., Krauss, R.M., Savage, P.J., Smith, S.C., Spertus, J.A., Fernando Costa, 2005. Diagnosis and management of the metabolic syndrome: an American Heart Association/National Heart, Lung, and Blood Institute scientific statement: Executive Summary. Crit Pathw Cardiol 4, 198–203. doi:10.1097/00132577-200512000-00018

Grzegorzewska, A.E., Niepolski, L., Świderska, M.K., Mostowska, A., Stolarek, I., Warchoł, W., Figlerowicz, M., Jagodziński, P.P., 2018. ENHO, RXRA, and LXRA polymorphisms and dyslipidaemia, related comorbidities and

survival in haemodialysis patients. BMC Med. Genet. 19, 194. doi:10.1186/s12881-018-0708-4

Guilherme, A., Henriques, F., Bedard, A.H., Czech, M.P., 2019. Molecular pathways linking adipose innervation to insulin action in obesity and diabetes mellitus. Nat Rev Endocrinol 15, 207–225. doi:10.1038/s41574-019-0165-y

Guo, L., Worth, A.J., Mesaros, C., Snyder, N.W., Glickson, J.D., Blair, I.A., 2016. Diisopropylethylamine/hexafluoroisopropanol-mediated ion-pairing ultra-high-performance liquid chromatography/mass spectrometry for phosphate and carboxylate metabolite analysis: utility for studying cellular metabolism. Rapid Commun. Mass Spectrom. 30, 1835–1845. doi:10.1002/rcm.7667

Hardy, O.T., Czech, M.P., Corvera, S., 2012. What causes the insulin resistance underlying obesity? Curr Opin Endocrinol Diabetes Obes 19, 81–87. doi:10.1097/MED.0b013e3283514e13

Heinrich, P.C., Behrmann, I., Haan, S., Hermanns, H.M., Müller-Newen, G., Schaper, F., 2003. Principles of interleukin (IL)-6-type cytokine signalling and its regulation. Biochem. J. 374, 1–20. doi:10.1042/BJ20030407

Hildrum, B., Mykletun, A., Dahl, A.A., Midthjell, K., 2009. Metabolic syndrome and risk of mortality in middle-aged versus elderly individuals: the Nord-Trøndelag Health Study (HUNT). Diabetologia 52, 583–590. doi:10.1007/s00125-009-1271-5

Hine, C., Harputlugil, E., Zhang, Y., Ruckenstuhl, C., Lee, B.C., Brace, L., Longchamp, A., Treviño-Villarreal, J.H., Mejia, P., Ozaki, C.K., Wang, R., Gladyshev, V.N., Madeo, F., Mair, W.B., Mitchell, J.R., 2015. Endogenous

hydrogen sulfide production is essential for dietary restriction benefits. Cell 160, 132–144. doi:10.1016/j.cell.2014.11.048

Houtkooper, R.H., Argmann, C., Houten, S.M., Cantó, C., Jeninga, E.H., Andreux, P.A., Thomas, C., Doenlen, R., Schoonjans, K., Auwerx, J., 2011. The metabolic footprint of aging in mice. Sci Rep 1, 134. doi:10.1038/srep00134

Hsieh, C.-C., Liao, C.-C., Liao, Y.-C., Hwang, L.S., Wu, L.-Y., Hsieh, S.-C., 2016. Proteomic changes associated with metabolic syndrome in a fructose-fed rat model. J Food Drug Anal 24, 754–761. doi:10.1016/j.jfda.2016.03.005

Hunter, G.R., Gower, B.A., Kane, B.L., 2010. Age Related Shift in Visceral Fat. Int J Body Compos Res 8, 103–108.

Kennedy, A.J., Ellacott, K.L.J., King, V.L., Hasty, A.H., 2010. Mouse models of the metabolic syndrome. Dis Model Mech 3, 156–166. doi:10.1242/dmm.003467

Kenyon, C.J., 2010. The genetics of ageing. Nature 464, 504–512. doi:10.1038/nature08980

Kotzbeck, P., Giordano, A., Mondini, E., Murano, I., Severi, I., Venema, W., Cecchini, M.P., Kershaw, E.E., Barbatelli, G., Haemmerle, G., Zechner, R., Cinti, S., 2018. Brown adipose tissue whitening leads to brown adipocyte death and adipose tissue inflammation. J. Lipid Res. 59, 784–794. doi:10.1194/jlr.M079665

Kõks, S., Dogan, S., Tuna, B.G., González-Navarro, H., Potter, P., Vandenbroucke, R.E., 2016. Mouse models of ageing and their relevance to disease. Mech. Ageing Dev. 160, 41–53. doi:10.1016/j.mad.2016.10.001

Kristensen, T., Fredholm, M., Cirera, S., 2015. Expression study of GLUT4 translocation-related genes in a porcine pre-diabetic model. Mamm. Genome 26, 650–657. doi:10.1007/s00335-015-9601-z

Kuskovsky, R., Buj, R., Xu, P., Hofbauer, S., Doan, M.T., Jiang, H., Bostwick, A., Mesaros, C., Aird, K.M., Snyder, N.W., 2019. Simultaneous isotope dilution quantification and metabolic tracing of deoxyribonucleotides by liquid chromatography high resolution mass spectrometry. Anal. Biochem. 568, 65–72. doi:10.1016/j.ab.2018.12.023

Landskron, G., la Fuente, De, M., Thuwajit, P., Thuwajit, C., Hermoso, M.A., 2014. Chronic inflammation and cytokines in the tumor microenvironment. J Immunol Res 2014, 149185. doi:10.1155/2014/149185

Lawson, B.R., Belkowski, S.M., Whitesides, J.F., Davis, P., Lawson, J.W., 2007. Immunomodulation of murine collagen-induced arthritis by N, N-dimethylglycine and a preparation of Perna canaliculus. BMC Complement Altern Med 7, 20. doi:10.1186/1472-6882-7-20

Lee, C.D., Longo, V.D., 2018. Growth Hormones and Aging

. Principles of Endocrinology and Hormone Action 691–702. doi:10.1007/978-3-319-44675-2_27

Leite, M.I., Jones, M., Ströbel, P., Marx, A., Gold, R., Niks, E., Verschuuren, J.J.G.M., Berrih-Aknin, S., Scaravilli, F., Canelhas, A., Morgan, B.P., Vincent, A., Willcox, N., 2007. Myasthenia gravis thymus: complement vulnerability of epithelial and myoid cells, complement attack on them, and correlations with autoantibody status. Am. J. Pathol. 171, 893–905. doi:10.2353/ajpath.2007.070240

Lewis, D.F.V., 2004. 57 varieties: the human cytochromes P450. Pharmacogenomics 5, 305–318. doi:10.1517/phgs.5.3.305.29827

Li, H., Auwerx, J., 2020. Mouse Systems Genetics as a Prelude to Precision Medicine. Trends Genet. doi:10.1016/j.tig.2020.01.004

Liao, C.-Y., Kennedy, B.K., 2014. Mouse models and aging: longevity and progeria. Curr. Top. Dev. Biol. 109, 249–285. doi:10.1016/B978-0-12-397920-9.00003-2

Liao, C.-Y., Rikke, B.A., Johnson, T.E., Diaz, V., Nelson, J.F., 2010. Genetic variation in the murine lifespan response to dietary restriction: from life extension to life shortening. Aging Cell 9, 92–95. doi:10.1111/j.1474-9726.2009.00533.x

Libby, P., 2002. Inflammation in atherosclerosis. Nature 420, 868–874. doi:10.1038/nature01323

Liberzon, A., Birger, C., Thorvaldsdóttir, H., Ghandi, M., Mesirov, J.P., Tamayo, P., 2015. The Molecular Signatures Database (MSigDB) hallmark gene set collection. Cell Syst 1, 417–425. doi:10.1016/j.cels.2015.12.004

Longo, V.D., Antebi, A., Bartke, A., Barzilai, N., Brown-Borg, H.M., Caruso, C., Curiel, T.J., de Cabo, R., Franceschi, C., Gems, D., Ingram, D.K., Johnson, T.E., Kennedy, B.K., Kenyon, C., Klein, S., Kopchick, J.J., Lepperdinger, G., Madeo, F., Mirisola, M.G., Mitchell, J.R., Passarino, G., Rudolph, K.L., Sedivy, J.M., Shadel, G.S., Sinclair, D.A., Spindler, S.R., Suh, Y., Vijg, J., Vinciguerra, M., Fontana, L., 2015. Interventions to Slow Aging in Humans: Are We Ready? Aging Cell 14, 497–510. doi:10.1111/acel.12338

Love, M.I., Huber, W., Anders, S., 2014. Moderated estimation of fold change and dispersion for RNA-seq data with DESeq2. Genome Biol. 15, 550. doi:10.1186/s13059-014-0550-8

López-Otín, C., Blasco, M.A., Partridge, L., Serrano, M., Kroemer, G., 2013. The hallmarks of aging. Cell 153, 1194–1217. doi:10.1016/j.cell.2013.05.039

López-Otín, C., Galluzzi, L., Freije, J.M.P., Madeo, F., Kroemer, G., 2016. Metabolic Control of Longevity. Cell 166, 802–821. doi:10.1016/j.cell.2016.07.031

Lund, J., Lund, C., Morville, T., Clemmensen, C., 2020. The unidentified hormonal defense against weight gain. PLoS Biol. 18, e3000629. doi:10.1371/journal.pbio.3000629

Maier, T., Güell, M., Serrano, L., 2009. Correlation of mRNA and protein in complex biological samples. FEBS Lett. 583, 3966–3973. doi:10.1016/j.febslet.2009.10.036

Malakouti, M., Kataria, A., Ali, S.K., Schenker, S., 2017. Elevated Liver Enzymes in Asymptomatic Patients - What Should I Do? J Clin Transl Hepatol 5, 394–403. doi:10.14218/JCTH.2017.00027

Meuwissen, T.H., 1997. Maximizing the response of selection with a predefined rate of inbreeding. J. Anim. Sci. 75, 934–940. doi:10.2527/1997.754934x

Miller, K.N., Burhans, M.S., Clark, J.P., Howell, P.R., Polewski, M.A., DeMuth, T.M., Eliceiri, K.W., Lindstrom, M.J., Ntambi, J.M., Anderson, R.M., 2017. Aging and caloric restriction impact adipose tissue, adiponectin, and circulating lipids. Aging Cell. doi:10.1111/acel.12575

Mohammadi, M., Gozashti, M.H., Aghadavood, M., Mehdizadeh, M.R., Hayatbakhsh, M.M., 2017. Clinical Significance of Serum IL-6 and TNF-α Levels in Patients with Metabolic Syndrome. Rep Biochem Mol Biol 6, 74–79.

Monteiro, R., Azevedo, I., 2010. Chronic inflammation in obesity and the metabolic syndrome. Mediators Inflamm. 2010. doi:10.1155/2010/289645

Morgan, E.T., 2009. Impact of infectious and inflammatory disease on cytochrome P450-mediated drug metabolism and pharmacokinetics. Clin. Pharmacol. Ther. 85, 434–438. doi:10.1038/clpt.2008.302

Nikolich-Žugich, J., Goldman, D.P., Cohen, P.R., Cortese, D., Fontana, L., Kennedy, B.K., Mohler, M.J., Olshansky, S.J., Perls, T., Perry, D., Richardson, A., Ritchie, C., Wertheimer, A.M., Faragher, R.G.A., Fain, M.J., 2016. Preparing for an Aging World: Engaging Biogerontologists, Geriatricians, and the Society., in:. Presented at the The journals of gerontology. Series A, Biological sciences and medical sciences, pp. 435–444. doi:10.1093/gerona/glv164

Obata, F., Kuranaga, E., Tomioka, K., Ming, M., Takeishi, A., Chen, C.-H., Soga, T., Miura, M., 2014. Necrosis-driven systemic immune response alters SAM metabolism through the FOXO-GNMT axis. Cell Rep 7, 821–833. doi:10.1016/j.celrep.2014.03.046

Obata, F., Miura, M., 2015. Enhancing S-adenosyl-methionine catabolism extends Drosophila lifespan. Nat Commun 6, 8332. doi:10.1038/ncomms9332

Pan, W., Chandalia, M., Abate, N., 2012. New Insights into the Role of ENPP1 in Insulin Resistance. J Metabonomics Metab 1. doi:10.4172/2325-9736.1000e103

Pearse, G., 2006. Histopathology of the thymus. Toxicol Pathol 34, 515–547. doi:10.1080/01926230600978458

Peleg, S., Feller, C., Forne, I., Schiller, E., Sévin, D.C., Schauer, T., Regnard, C., Straub, T., Prestel, M., Klima, C., Schmitt Nogueira, M., Becker, L., Klopstock, T., Sauer, U., Becker, P.B., Imhof, A., Ladurner, A.G., 2016a. Life span extension by targeting a link between metabolism and histone acetylation in Drosophila. EMBO Rep. 17, 455–469. doi:10.15252/embr.201541132

Peleg, S., Feller, C., Ladurner, A.G., Imhof, A., 2016b. The Metabolic Impact on Histone Acetylation and Transcription in Ageing. Trends Biochem. Sci. 41, 700–711. doi:10.1016/j.tibs.2016.05.008

Poeschla, M., Valenzano, D.R., 2020. The turquoise killifish: a genetically tractable model for the study of aging. J. Exp. Biol. 223. doi:10.1242/jeb.209296

Poiley, S.M., 1960. A systematic method of breeder rotation for non-inbred laboratory animal colonies. Proc Anim Care Panel 159–166.

Popko, K., Gorska, E., Stelmaszczyk-Emmel, A., Plywaczewski, R., Stoklosa, A., Gorecka, D., Pyrzak, B., Demkow, U., 2010. Proinflammatory cytokines Il-6 and TNF-α and the development of inflammation in obese subjects. Eur. J. Med. Res. 15 Suppl 2, 120–122. doi:10.1186/2047-783x-15-s2-120

Pradhan, A.D., Manson, J.E., Rifai, N., Buring, J.E., Ridker, P.M., 2001. C-reactive protein, interleukin 6, and risk of developing type 2 diabetes mellitus. JAMA 286, 327–334. doi:10.1001/jama.286.3.327

Puca, A.A., Chatgilialoglu, C., Ferreri, C., 2008. Lipid metabolism and diet: possible mechanisms of slow aging. Int. J. Biochem. Cell Biol. 40, 324–333. doi:10.1016/j.biocel.2007.04.003

Rathkolb, B., Hans, W., Prehn, C., Fuchs, H., Gailus-Durner, V., Aigner, B., Adamski, J., Wolf, E., Hrabe de Angelis, M., 2013. Clinical Chemistry and Other Laboratory Tests on Mouse Plasma or Serum. Curr Protoc Mouse Biol 3, 69–100. doi:10.1002/9780470942390.mo130043

Renne, U., Langhammer, M., Brenmoehl, J., Walz, C., Zeissler, A., Tuchscherer, A., Piechotta, M., Wiesner, R.J., Bielohuby, M., Hoeflich, A., 2013. Lifelong obesity in a polygenic mouse model prevents age- and diet-induced glucose intolerance- obesity is no road to late-onset diabetes in mice. PLoS ONE 8, e79788. doi:10.1371/journal.pone.0079788

Ridker, P.M., Everett, B.M., Thuren, T., MacFadyen, J.G., Chang, W.H., Ballantyne, C., Fonseca, F., Nicolau, J., Koenig, W., Anker, S.D., Kastelein, J.J.P., Cornel, J.H., Pais, P., Pella, D., Genest, J., Cifkova, R., Lorenzatti, A., Forster, T., Kobalava, Z., Vida-Simiti, L., Flather, M., Shimokawa, H., Ogawa, H., Dellborg, M., Rossi, P.R.F., Troquay, R.P.T., Libby, P., Glynn, R.J., CANTOS Trial Group, 2017. Antiinflammatory Therapy with Canakinumab for Atherosclerotic Disease. N. Engl. J. Med. 377, 1119–1131. doi:10.1056/NEJMoa1707914

Ritchie, M.E., Phipson, B., Wu, D., Hu, Y., Law, C.W., Shi, W., Smyth, G.K., 2015. limma powers differential expression analyses for RNA-sequencing

and microarray studies. Nucleic Acids Res. 43, e47. doi:10.1093/nar/gkv007

Rozman, J., Rathkolb, B., Neschen, S., Fuchs, H., Gailus-Durner, V., Klingenspor, M., Wolf, E., Hrabe de Angelis, M., 2015. Glucose tolerance tests for systematic screening of glucose homeostasis in mice. Curr Protoc Mouse Biol 5, 65–84. doi:10.1002/9780470942390.mo140111

Saltiel, A.R., Kahn, C.R., 2001. Insulin signalling and the regulation of glucose and lipid metabolism. Nature 414, 799–806. doi:10.1038/414799a

Samokhvalov, V., Ussher, J.R., Fillmore, N., Armstrong, I.K.G., Keung, W., Moroz, D., Lopaschuk, D.G., Seubert, J., Lopaschuk, G.D., 2012. Inhibition of malonyl-CoA decarboxylase reduces the inflammatory response associated with insulin resistance. Am. J. Physiol. Endocrinol. Metab. 303, E1459–68. doi:10.1152/ajpendo.00018.2012

Schüler, L., 1985. Selection for fertility in mice - the selection plateau and how to overcome it. Theor. Appl. Genet. 70, 72–79. doi:10.1007/BF00264485

Selman, C., Nussey, D.H., Monaghan, P., 2013. Ageing: it"s a dog"s life. Curr. Biol. 23, R451–3. doi:10.1016/j.cub.2013.04.005

Senjo, H., Higuchi, T., Okada, S., Takahashi, O., 2018. Hyperferritinemia: causes and significance in a general hospital. Hematology 23, 817–822. doi:10.1080/10245332.2018.1488569

Shah, R.V., Murthy, V.L., Abbasi, S.A., Blankstein, R., Kwong, R.Y., Goldfine, A.B., Jerosch-Herold, M., Lima, J.A.C., Ding, J., Allison, M.A., 2014. Visceral adiposity and the risk of metabolic syndrome across body mass index: the MESA Study. JACC Cardiovasc Imaging 7, 1221–1235. doi:10.1016/j.jcmg.2014.07.017

Siewert, E., Bort, R., Kluge, R., Heinrich, P.C., Castell, J., Jover, R., 2000. Hepatic cytochrome P450 down-regulation during aseptic inflammation in the mouse is interleukin 6 dependent. Hepatology 32, 49–55. doi:10.1053/jhep.2000.8532

Steger, R.W., Bartke, A., Cecim, M., 1993. Premature ageing in transgenic mice expressing different growth hormone genes. J. Reprod. Fertil. Suppl. 46, 61–75.

Stepanova, M., Rodriguez, E., Birerdinc, A., Baranova, A., 2015. Age-independent rise of inflammatory scores may contribute to accelerated aging in multi-morbidity. Oncotarget 6, 1414–1421. doi:10.18632/oncotarget.2725

Timtchenko, D., Kratzsch, J., Sauerwein, H., Wegner, J., Souffrant, W.B., Schwerin, M., Brockmann, G.A., 1999. Fat storage capacity in growth-selected and control mouse lines is associated with line-specific gene expression and plasma hormone levels. Int. J. Obes. Relat. Metab. Disord. 23, 586–594.

Tyanova, S., Temu, T., Cox, J., 2016. The MaxQuant computational platform for mass spectrometry-based shotgun proteomics. Nat Protoc 11, 2301–2319. doi:10.1038/nprot.2016.136

Ussher, J.R., Fillmore, N., Keung, W., Zhang, L., Mori, J., Sidhu, V.K., Fukushima, A., Gopal, K., Lopaschuk, D.G., Wagg, C.S., Jaswal, J.S., Dyck, J.R.B., Lopaschuk, G.D., 2016. Genetic and Pharmacological Inhibition of Malonyl CoA Decarboxylase Does Not Exacerbate Age-Related Insulin Resistance in Mice. Diabetes 65, 1883–1891. doi:10.2337/db15-1145

Ward, J.M., Rehg, J.E., Morse, H.C., 2012. Differentiation of rodent immune and hematopoietic system reactive lesions from neoplasias. Toxicol Pathol 40, 425–434. doi:10.1177/0192623311431467

Weiss, T.W., Arnesen, H., Seljeflot, I., 2013. Components of the interleukin-6 transsignalling system are associated with the metabolic syndrome, endothelial dysfunction and arterial stiffness. Metab. Clin. Exp. 62, 1008–1013. doi:10.1016/j.metabol.2013.01.019

WHO, 2020. Obesity and Overweight Factsheet.

Wilcox, G., 2005. Insulin and insulin resistance. Clin Biochem Rev 26, 19–39.

Yan, H., Xia, M., Chang, X., Xu, Q., Bian, H., Zeng, M., Rao, S., Yao, X., Tu, Y., Jia, W., Gao, X., 2011. Circulating fibroblast growth factor 21 levels are closely associated with hepatic fat content: a cross-sectional study. PLoS ONE 6, e24895. doi:10.1371/journal.pone.0024895

Yu, G., Wang, L.-G., Han, Y., He, Q.-Y., 2012. clusterProfiler: an R package for comparing biological themes among gene clusters. OMICS 16, 284–287. doi:10.1089/omi.2011.0118

Yuan, R., Tsaih, S.-W., Petkova, S.B., Marin de Evsikova, C., Xing, S., Marion, M.A., Bogue, M.A., Mills, K.D., Peters, L.L., Bult, C.J., Rosen, C.J., Sundberg, J.P., Harrison, D.E., Churchill, G.A., Paigen, B., 2009. Aging in inbred strains of mice: study design and interim report on median lifespans and circulating IGF1 levels. Aging Cell 8, 277–287. doi:10.1111/j.1474-9726.2009.00478.x

Zannis, V.I., Fotakis, P., Koukos, G., Kardassis, D., Ehnholm, C., Jauhiainen, M., Chroni, A., 2015. HDL biogenesis, remodeling, and catabolism. Handb Exp Pharmacol 224, 53–111. doi:10.1007/978-3-319-09665-0_2

Zhang, X., Yeung, D.C.Y., Karpisek, M., Stejskal, D., Zhou, Z.-G., Liu, F., Wong, R.L.C., Chow, W.-S., Tso, A.W.K., Lam, K.S.L., Xu, A., 2008. Serum FGF21 levels are increased in obesity and are independently associated with the metabolic syndrome in humans. Diabetes 57, 1246–1253. doi:10.2337/db07-1476

Zhang, Y., Proenca, R., Maffei, M., Barone, M., Leopold, L., Friedman, J.M., 1994. Positional cloning of the mouse obese gene and its human homologue. Nature 372, 425–432. doi:10.1038/372425a0

Zoico, E., Rubele, S., De Caro, A., Nori, N., Mazzali, G., Fantin, F., Rossi, A., Zamboni, M., 2019. Brown and Beige Adipose Tissue and Aging. Front Endocrinol (Lausanne) 10, 368. doi:10.3389/fendo.2019.00368

Figure 1

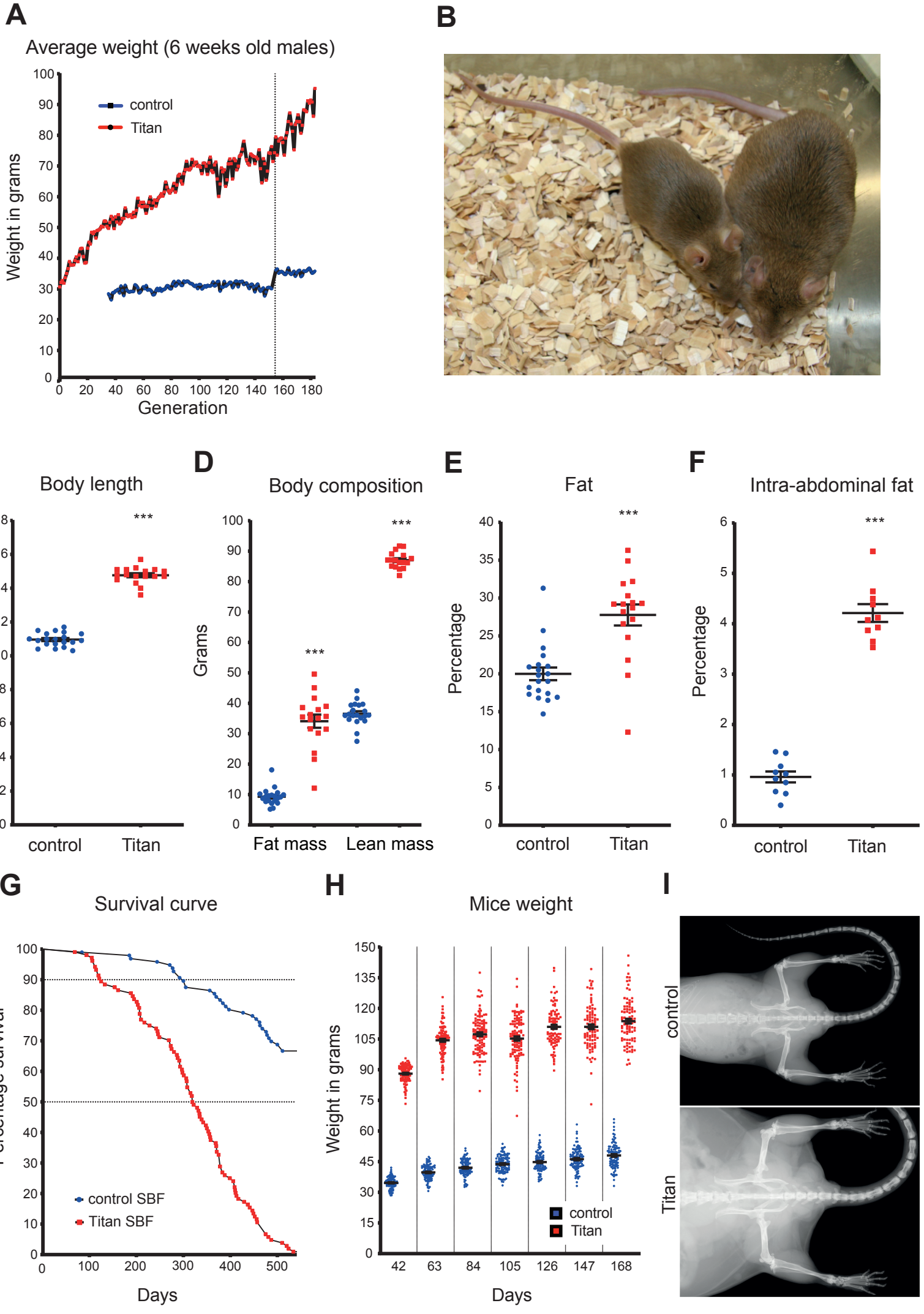

Figure 2

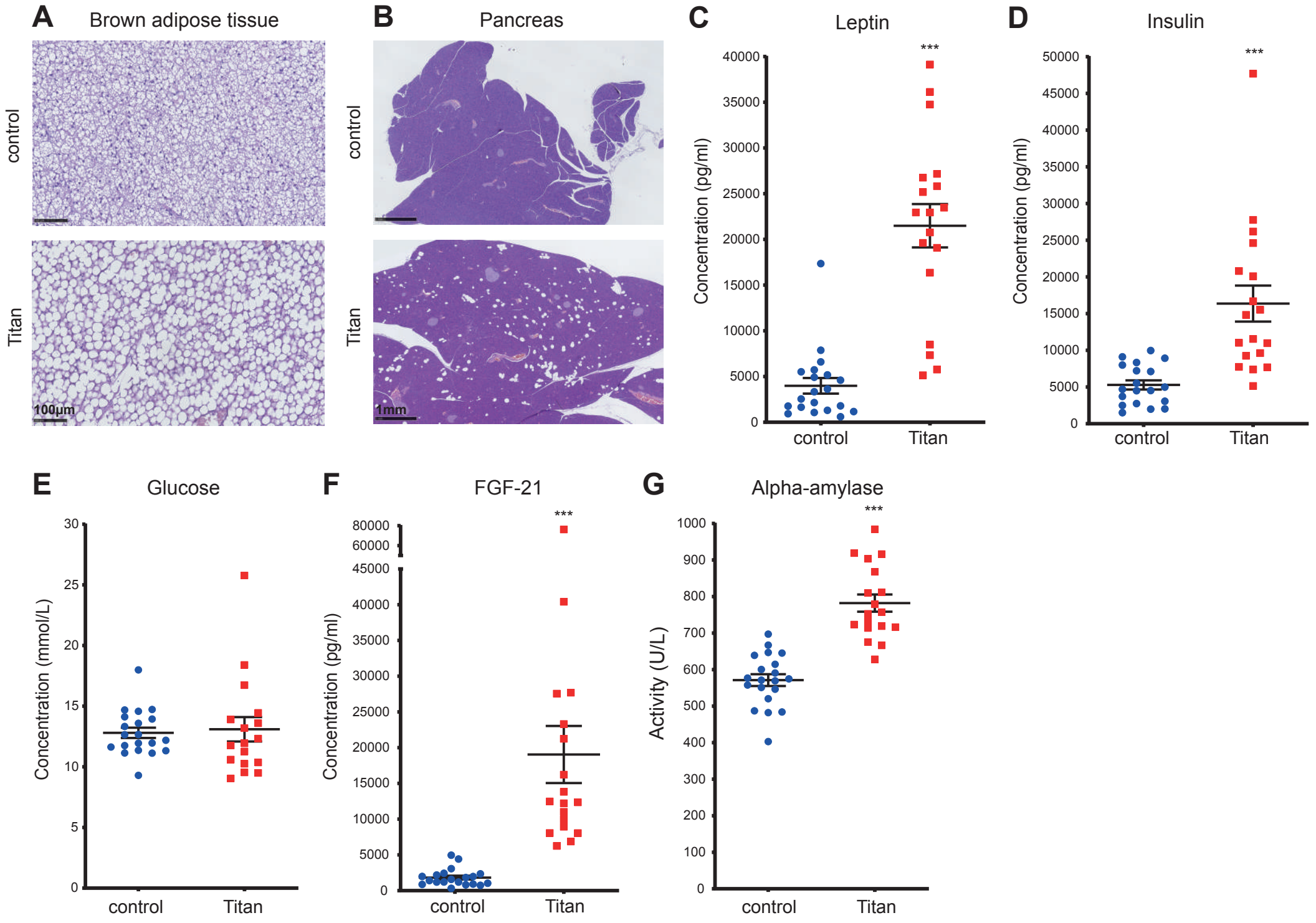
A
Brown adipose tissue
control
Titan
100µm
B
Pancreas
control
Titan
1mm
C
Leptin
Concentration (pg/ml)
***
control
Titan
D
Insulin
Concentration (pg/ml)
***
control
Titan
E
Glucose
Concentration (mmol/L)
control
Titan
F
FGF-21
Concentration (pg/ml)
***
control
Titan
G
Alpha-amylase
Activity (U/L)
***
control
Titan

Figure 3

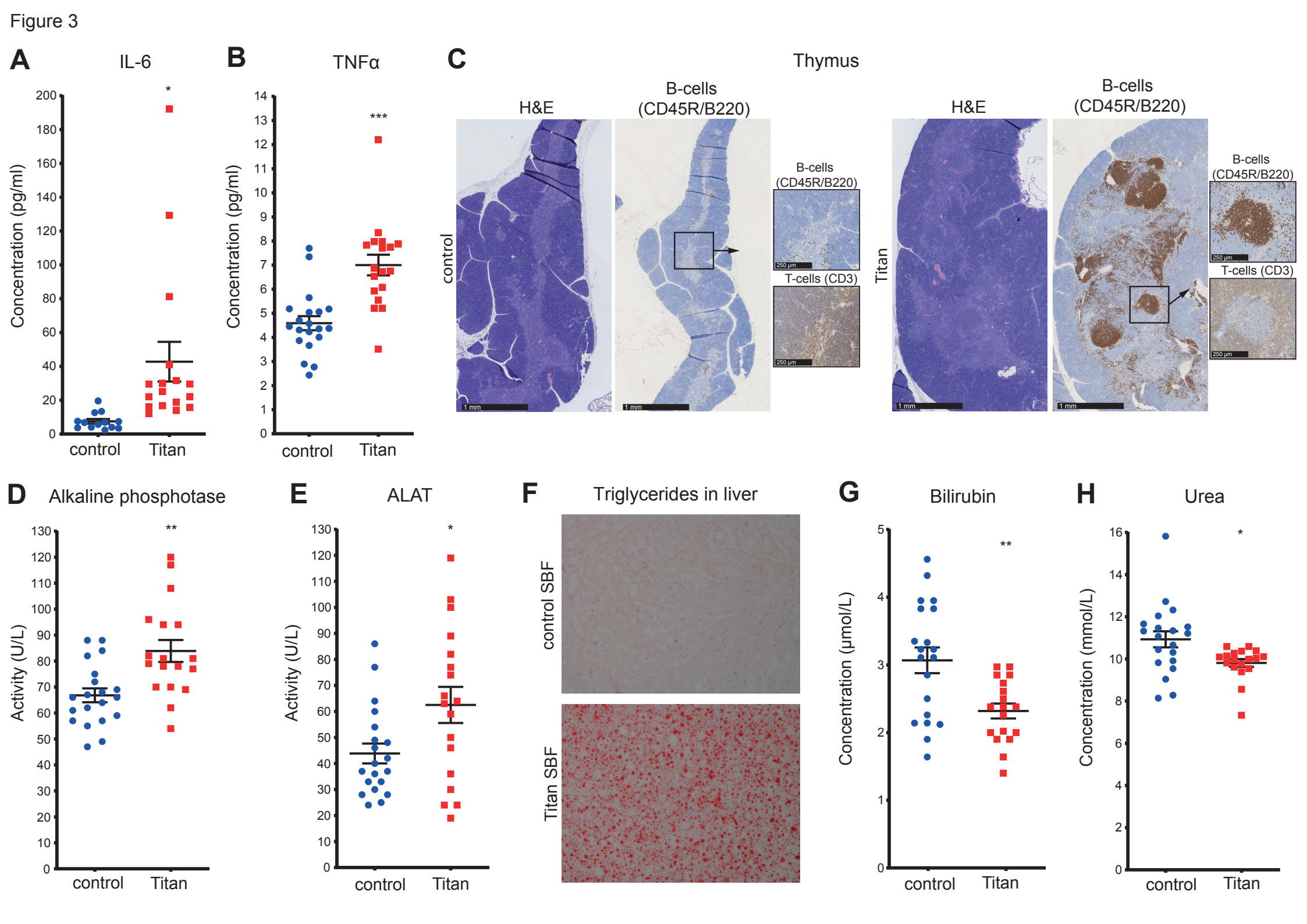
A
IL-6
Concentration (pg/ml)
control
Titan
B
TNFα
Concentration (pg/ml)
control
Titan
C
Thymus
H&E
B-cells (CD45R/B220)
control
B-cells (CD45R/B220)
T-cells (CD3)
Titan
D
Alkaline phosphotase
Activity (U/L)
control
Titan
E
ALAT
Activity (U/L)
control
Titan
F
Triglycerides in liver
control SBF
Titan SBF
G
Bilirubin
Concentration (µmol/L)
control
Titan
H
Urea
Concentration (mmol/L)
control
Titan

Figure 4

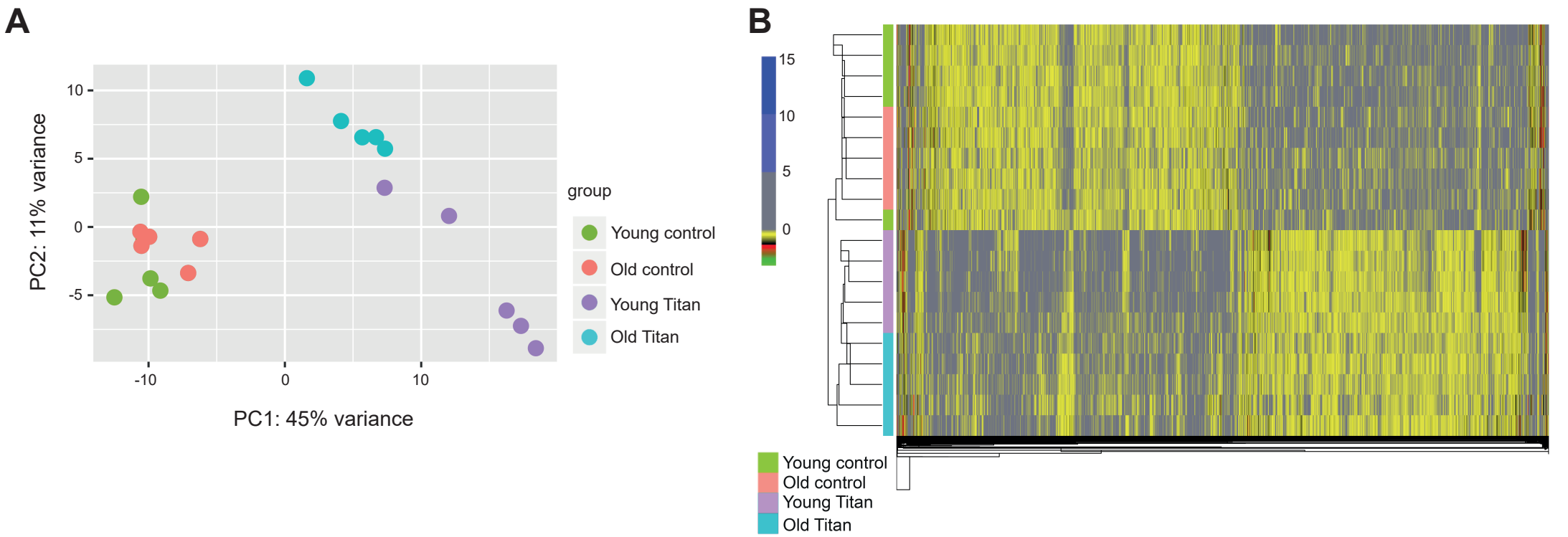
A
PC2: 11% variance
PC1: 45% variance
group
Young control
Old control
Young Titan
Old Titan
B
Young control
Old control
Young Titan
Old Titan
C
Younger
Upregulated
Downregulated
GO Term
-log10(p.adjust)
D
Older
Upregulated
Downregulated
GO Term
-log10(p.adjust)

Figure 5

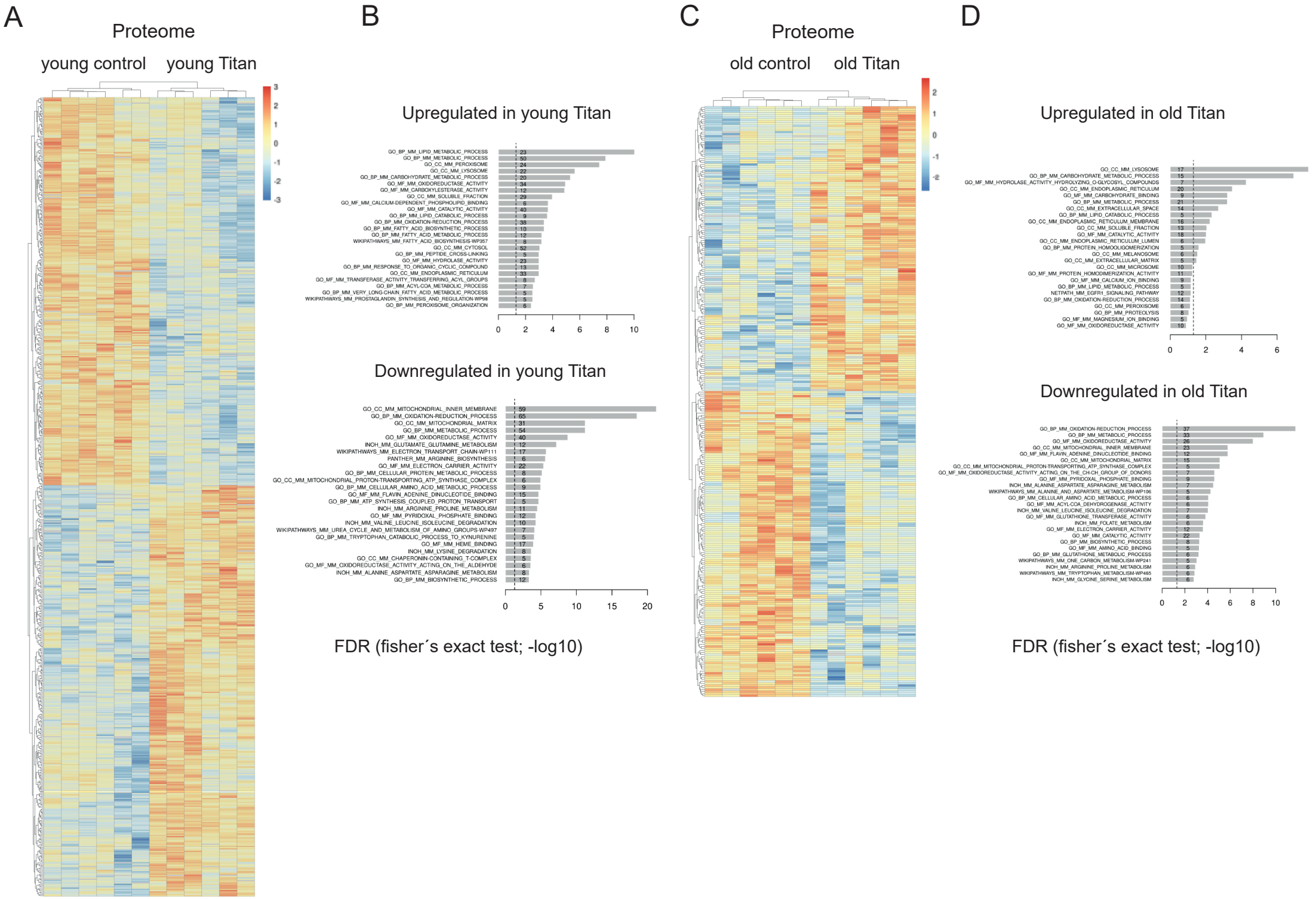
A
Proteome
young control
young Titan
B
Upregulated in young Titan
GO_BP_MM_LIPID_METABOLIC_PROCESS 23
GO_BP_MM_METABOLIC_PROCESS 50
GO_CC_MM_PEROXISOME 24
GO_CC_MM_LYSOSOME 22
GO_BP_MM_CARBOHYDRATE_METABOLIC_PROCESS 20
GO_MF_MM_OXIDOREDUCTASE_ACTIVITY 34
GO_MF_MM_CARBOXYLESTERASE_ACTIVITY 12
GO_CC_MM_SOLUBLE_FRACTION 29
GO_MF_MM_CALCIUM-DEPENDENT_PHOSPHOLIPID_BINDING 6
GO_MF_MM_CATALYTIC_ACTIVITY 40
GO_BP_MM_LIPID_CATABOLIC_PROCESS 9
GO_BP_MM_OXIDATION-REDUCTION_PROCESS 38
GO_BP_MM_FATTY_ACID_BIOSYNTHETIC_PROCESS 10
GO_BP_MM_FATTY_ACID_METABOLIC_PROCESS 12
WIKIPATHWAYS_MM_FATTY_ACID_BIOSYNTHESIS-WP357 8
GO_CC_MM_CYTOSOL 52
GO_BP_MM_PEPTIDE_CROSS-LINKING 5
GO_MF_MM_HYDROLASE_ACTIVITY 23
GO_BP_MM_RESPONSE_TO_ORGANIC_CYCLIC_COMPOUND 13
GO_CC_MM_ENDOPLASMIC_RETICULUM 33
GO_MF_MM_TRANSFERASE_ACTIVITY_TRANSFERRING_ACYL_GROUPS 8
GO_BP_MM_ACYL-COA_METABOLIC_PROCESS 7
GO_BP_MM_VERY_LONG-CHAIN_FATTY_ACID_METABOLIC_PROCESS 5
WIKIPATHWAYS_MM_PROSTAGLANDIN_SYNTHESIS_AND_REGULATION-WP98 5
GO_BP_MM_PEROXISOME_ORGANIZATION 6
0 2 4 6 8 10
Downregulated in young Titan
GO_CC_MM_MITOCHONDRIAL_INNER_MEMBRANE 59
GO_BP_MM_OXIDATION-REDUCTION_PROCESS 65
GO_CC_MM_MITOCHONDRIAL_MATRIX 31
GO_BP_MM_METABOLIC_PROCESS 54
GO_MF_MM_OXIDOREDUCTASE_ACTIVITY 40
INOH_MM_GLUTAMATE_GLUTAMINE_METABOLISM 12
WIKIPATHWAYS_MM_ELECTRON_TRANSPORT_CHAIN-WP111 17
PANTHER_MM_ARGININE_BIOSYNTHESIS 6
GO_MF_MM_ELECTRON_CARRIER_ACTIVITY 22
GO_BP_MM_CELLULAR_PROTEIN_METABOLIC_PROCESS 8
GO_CC_MM_MITOCHONDRIAL_PROTON-TRANSPORTING_ATP_SYNTHASE_COMPLEX 6
GO_BP_MM_CELLULAR_AMINO_ACID_METABOLIC_PROCESS 9
GO_MF_MM_FLAVIN_ADENINE_DINUCLEOTIDE_BINDING 15
GO_BP_MM_ATP_SYNTHESIS_COUPLED_PROTON_TRANSPORT 5
INOH_MM_ARGININE_PROLINE_METABOLISM 11
GO_MF_MM_PYRIDOXAL_PHOSPHATE_BINDING 12
INOH_MM_VALINE_LEUCINE_ISOLEUCINE_DEGRADATION 10
WIKIPATHWAYS_MM_UREA_CYCLE_AND_METABOLISM_OF_AMINO_GROUPS-WP497 7
GO_BP_MM_TRYPTOPHAN_CATABOLIC_PROCESS_TO_KYNURENINE 5
GO_MF_MM_HEME_BINDING 17
INOH_MM_LYSINE_DEGRADATION 8
GO_CC_MM_CHAPERONIN-CONTAINING_T-COMPLEX 5
GO_MF_MM_OXIDOREDUCTASE_ACTIVITY_ACTING_ON_THE_ALDEHYDE 6
INOH_MM_ALANINE_ASPARTATE_ASPARAGINE_METABOLISM 8
GO_BP_MM_BIOSYNTHETIC_PROCESS 12
0 5 10 15 20
FDR (fisher´s exact test; -log10)
C
Proteome
old control
old Titan
D
Upregulated in old Titan
GO_CC_MM_LYSOSOME 17
GO_BP_MM_CARBOHYDRATE_METABOLIC_PROCESS 15
GO_MF_MM_HYDROLASE_ACTIVITY_HYDROLYZING_O-GLYCOSYL_COMPOUNDS 7
GO_CC_MM_ENDOPLASMIC_RETICULUM 20
GO_MF_MM_CARBOHYDRATE_BINDING 9
GO_BP_MM_METABOLIC_PROCESS 21
GO_CC_MM_EXTRACELLULAR_SPACE 14
GO_BP_MM_LIPID_CATABOLIC_PROCESS 5
GO_CC_MM_ENDOPLASMIC_RETICULUM_MEMBRANE 16
GO_CC_MM_SOLUBLE_FRACTION 13
GO_MF_MM_CATALYTIC_ACTIVITY 18
GO_CC_MM_ENDOPLASMIC_RETICULUM_LUMEN 6
GO_BP_MM_PROTEIN_HOMOOLIGOMERIZATION 5
GO_CC_MM_MELANOSOME 6
GO_CC_MM_EXTRACELLULAR_MATRIX 5
GO_CC_MM_MICROSOME 10
GO_MF_MM_PROTEIN_HOMODIMERIZATION_ACTIVITY 11
GO_MF_MM_CALCIUM_ION_BINDING 9
GO_BP_MM_LIPID_METABOLIC_PROCESS 5
NETPATH_MM_EGFR1_SIGNALING_PATHWAY 12
GO_BP_MM_OXIDATION-REDUCTION_PROCESS 14
GO_CC_MM_PEROXISOME 6
GO_BP_MM_PROTEOLYSIS 8
GO_MF_MM_MAGNESIUM_ION_BINDING 5
GO_MF_MM_OXIDOREDUCTASE_ACTIVITY 10
0 2 4 6
Downregulated in old Titan
GO_BP_MM_OXIDATION-REDUCTION_PROCESS 37
GO_BP_MM_METABOLIC_PROCESS 33
GO_MF_MM_OXIDOREDUCTASE_ACTIVITY 26
GO_CC_MM_MITOCHONDRIAL_INNER_MEMBRANE 23
GO_MF_MM_FLAVIN_ADENINE_DINUCLEOTIDE_BINDING 12
GO_CC_MM_MITOCHONDRIAL_MATRIX 15
GO_CC_MM_MITOCHONDRIAL_PROTON-TRANSPORTING_ATP_SYNTHASE_COMPLEX 5
GO_MF_MM_OXIDOREDUCTASE_ACTIVITY_ACTING_ON_THE_CH-CH_GROUP_OF_DONORS 7
GO_MF_MM_PYRIDOXAL_PHOSPHATE_BINDING 9
INOH_MM_ALANINE_ASPARTATE_ASPARAGINE_METABOLISM 7
WIKIPATHWAYS_MM_ALANINE_AND_ASPARTATE_METABOLISM-WP106 5
GO_BP_MM_CELLULAR_AMINO_ACID_METABOLIC_PROCESS 6
GO_MF_MM_ACYL-COA_DEHYDROGENASE_ACTIVITY 6
INOH_MM_VALINE_LEUCINE_ISOLEUCINE_DEGRADATION 7
GO_MF_MM_GLUTATHIONE_TRANSFERASE_ACTIVITY 6
INOH_MM_FOLATE_METABOLISM 6
GO_MF_MM_ELECTRON_CARRIER_ACTIVITY 12
GO_MF_MM_CATALYTIC_ACTIVITY 22
GO_BP_MM_BIOSYNTHETIC_PROCESS 8
GO_MF_MM_AMINO_ACID_BINDING 5
GO_BP_MM_GLUTATHIONE_METABOLIC_PROCESS 6
WIKIPATHWAYS_MM_ONE_CARBON_METABOLISM-WP241 5
INOH_MM_ARGININE_PROLINE_METABOLISM 6
WIKIPATHWAYS_MM_TRYPTOPHAN_METABOLISM-WP465 6
INOH_MM_GLYCINE_SERINE_METABOLISM 6
0 2 4 6 8 10
FDR (fisher´s exact test; -log10)

Figure 6

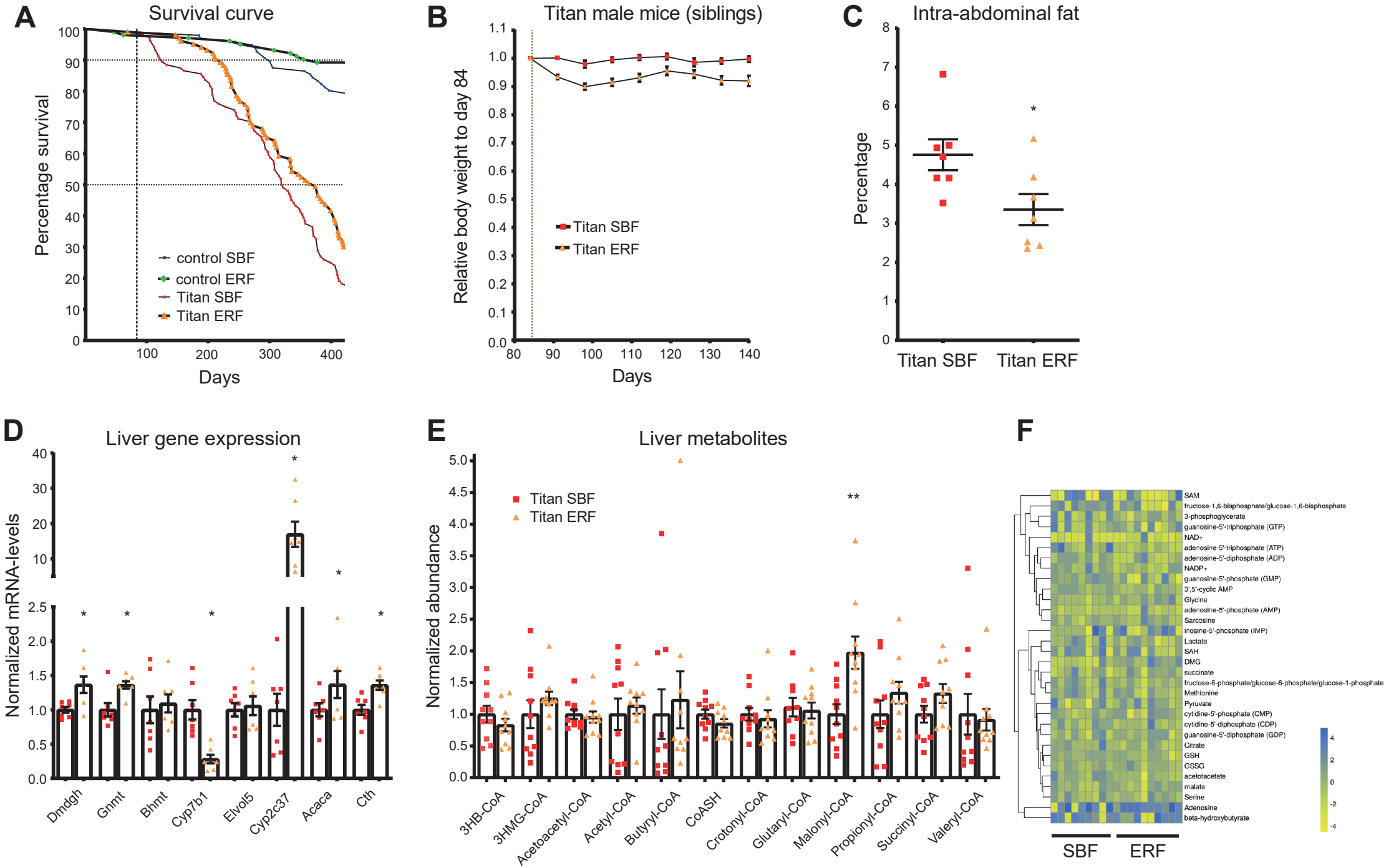
A
Survival curve
Percentage survival
Days
control SBF
control ERF
Titan SBF
Titan ERF
B
Titan male mice (siblings)
Relative body weight to day 84
Days
Titan SBF
Titan ERF
C
Intra-abdominal fat
Percentage
Titan SBF
Titan ERF
D
Liver gene expression
Normalized mRNA-levels
Dmdgh
Gnmt
Bhmt
Cyp7b1
Elvol5
Cyp2c37
Acaca
Cth
E
Liver metabolites
Normalized abundance
Titan SBF
Titan ERF
3HB-CoA
3HMG-CoA
Acetoacetyl-CoA
Acetyl-CoA
Butyryl-CoA
CoASH
Crotonyl-CoA
Glutaryl-CoA
Malonyl-CoA
Propionyl-CoA
Succinyl-CoA
Valeryl-CoA
F
SAM
fructose-1,6-bisphosphate/glucose-1,6-bisphosphate
3-phosphoglycerate
guanosine-5'-triphosphate (GTP)
NAD+
adenosine-5'-triphosphate (ATP)
adenosine-5'-diphosphate (ADP)
NADP+
guanosine-5'-phosphate (GMP)
3',5'-cyclic AMP
Glycine
adenosine-5'-phosphate (AMP)
Sarcosine
inosine-5'-phosphate (IMP)
Lactate
SAH
DMG
succinate
fructose-6-phosphate/glucose-6-phosphate/glucose-1-phosphate
Methionine
Pyruvate
cytidine-5'-phosphate (CMP)
cytidine-5'-diphosphate (CDP)
guanosine-5'-diphosphate (GDP)
Citrate
GSH
GSSG
acetotacetate
malate
Serine
Adenosine
beta-hydroxybutyrate
SBF
ERF